



**HAL**  
open science

# A CHIMERA MODEL FOR MOTION ANTICIPATION IN THE RETINA AND THE PRIMARY VISUAL CORTEX

Jérôme Emonet, Selma Souihel, Matteo Di Volo, Alain Destexhe, Frédéric  
Chavane, Bruno Cessac

► **To cite this version:**

Jérôme Emonet, Selma Souihel, Matteo Di Volo, Alain Destexhe, Frédéric Chavane, et al.. A  
CHIMERA MODEL FOR MOTION ANTICIPATION IN THE RETINA AND THE PRIMARY  
VISUAL CORTEX. 2024. hal-04709925

**HAL Id: hal-04709925**

**<https://inria.hal.science/hal-04709925v1>**

Preprint submitted on 26 Sep 2024

**HAL** is a multi-disciplinary open access archive for the deposit and dissemination of scientific research documents, whether they are published or not. The documents may come from teaching and research institutions in France or abroad, or from public or private research centers.

L'archive ouverte pluridisciplinaire **HAL**, est destinée au dépôt et à la diffusion de documents scientifiques de niveau recherche, publiés ou non, émanant des établissements d'enseignement et de recherche français ou étrangers, des laboratoires publics ou privés.



Distributed under a Creative Commons Attribution - NonCommercial 4.0 International License

---

# A CHIMERA MODEL FOR MOTION ANTICIPATION IN THE RETINA AND THE PRIMARY VISUAL CORTEX

---

## **Jerome Emonet**

Université Côte d'Azur, Inria  
Biovision team and Neuromod Institute  
Sophia Antipolis, France  
jerome.emonet@inria.fr

## **Selma Souihel**

P16 - Programme IA  
Inria Rocquencourt  
Domaine de Voluceau  
78150 Le Chesnay-Rocquencourt  
selma.souihel@inria.fr

## **Matteo di Volo**

Université Claude Bernard Lyon 1  
Institut National de la Santé et de la Recherche Médicale,  
Stem Cell and Brain Research Institute U1208  
Bron, France  
matteo.di-volo@univ-lyon1.fr

## **Alain Destexhe**

Institut NeuroPSI - UMR9197  
CNRS Paris-Saclay University  
Campus CEA Saclay, Saclay, FRANCE  
Alain.Destexhe@cnrns.fr

## **Frederic Chavane**

Institut de Neurosciences de la Timone UMR7289  
CNRS Aix-Marseille University  
13385 Marseille Cedex 05, France  
frederic.chavane@univ-amu.fr

## **Bruno Cessac**

Université Côte d'Azur, Inria  
Biovision team and Neuromod Institute  
Sophia Antipolis, France  
bruno.cessac@inria.fr

September 26, 2024

## **ABSTRACT**

We study motion anticipation in a mean field model of the primary visual cortex (V1) with a realistic retinal input. We assess the ability of this integrated retino-cortical model to reproduce experimental results on voltage dye optical imaging (VSDI) signal, in terms of two main quantities used to quantify anticipation: the latency and the time to peak. We unravel the effect of the stimulus features such as speed and contrast on anticipation. In addition, we explore the changes in the cortical wave of activation when V1 is driven by a retina output implementing different potential retina-driven anticipatory mechanisms, including gain control and lateral inhibition by amacrine cells.

**Keywords** Visual processing · Anticipation · Retina · V1 · Lateral connectivity

## **1 Introduction**

The brain is not just a reactive encoder, it is able to respond in a proactive way, especially with regards to stimuli. In visual processing, it is able to extrapolate and estimate how the visual stimulus is the most likely to behave in a near future, given the information of the past. This is, of course, based on the assumption that the stimulus is predictable to some extent. In particular, several studies have suggested that the predictability of stimuli can be learned from spatial and temporal regularities, arising e.g. in a deterministic trajectory. However, one can ask at which stage of the visual system do these predictions start taking place. At the level of the early stages of the visual system ? Or in late-stage processors ?

Prediction is a rather wide concept. If by this term, one refers to motion extrapolation, studies have reported that it already starts at the level of the retina. Berry et al. [1] have first shown that local gain control mechanisms, occurring at

the level of retinal bipolar and ganglion cells, can explain a form of local anticipation for a moving bar, by advancing the peak in the retinal ganglion cells response. This explains the change in the shape of response observed in experimental data - bringing the ganglion cells to their activity peak earlier than when they respond to a flashed bar - without modifying the time at which their activity starts increasing, i.e. when the bar enters in their receptive field. Another study by Johnston et al. [2] has emphasized the role of lateral inhibition in the elicitation of anticipatory mechanisms at the retinal level. They have proposed that motion anticipation can be mediated via feed-forward inhibition from amacrine cells inputs that specifically suppress the response to the moving object in the latter half of the receptive field. This mechanism as well truncates the response and yields an early response peak. According to the authors, this "adaptation anticipation" occurs at the level of synapses. It requires each excitatory synapse to be more distal than an inhibitory synapse on the pathway. The latter will inhibit its EPSP and generate a shift forward (anticipation) of the peak. Thus, there must be an excess of inhibitory synapses compared to excitatory ones. In this case, motion anticipation arises from the general properties of the retina connectome and from the feedforward inhibition that ganglion cells receive from amacrine cells. Souihel and Cessac [3] explored, in a modelling study, another potential anticipatory effect of amacrine cells. In addition to the feed-forward effects discussed in [2] feedback inhibition due to amacrine cells could induce a wave of activity further anticipating the bipolar cell response and thereby enhancing the effect of gain control. Finally, Menz et al [4] observed that motion anticipation can, in addition to a peak advancement by truncation of the response, arise by advancing the *onset* of the response, with a strong anticipatory effect. They hypothesize that this effect may come from amacrine cells: hyper-polarizing these cells would provide a dis-inhibitory input to ganglion cells prior to the object crossing the receptive field center.

It has also been shown that anticipation is further carried out at the level of the primary visual cortex [5, 6, 7, 8]. Jancke et al. [5] first demonstrated the existence of anticipatory mechanisms in the cat primary visual cortex. They recorded cells in the central visual field of area 17 of anesthetized cats, responding to small squares of light, either flashed or moving in different directions, and with different speeds. When presented with the moving stimulus, these cells show a reduction of neural latencies, as compared to the flashed stimulus. Subramaniyan et al. [7] have reported the existence of similar anticipatory effects in the macaque primary visual cortex, showing that a moving bar is processed faster than a flashed bar. They give two possible explanations to this phenomenon : either a shift in the cells receptive fields, induced by motion, or a faster propagation of motion signals. Consistent with the study by Jancke et al., they reported a speed dependence of the response latency as well as a luminance dependence. However, Subramaniyan et al. note that the motion representation delays are not reduced to zero, irrespective of the experimental setting of the flash lag effect. As a consequence, moving objects representation in V1 should be mislocalized. This observation is in favor of a collaborative work conducted, on the one hand, by the retina and V1 to help reducing the latencies, and, on the other hand, by other specialized brain regions which carry out predictive computations. Learning and training seem also to play important roles in calibrating the response of the nervous system to a given moving object. Finally, Benvenuti et al. [6, 8] have studied the trajectory-based activity in V1. They have compared voltage sensitive dye imaging responses for different cortical locations along a bar trajectory. By centering all positions on the same relative time events (bar centered in the middle of the receptive field), they have highlighted a gradient in the response (see also Fig. 2). The further the bar starts from the current position of a cortical column the earlier its activity rises. They gave convincing arguments that this increase is carried by the lateral connectivity in the cortex.

At the current state of the art there are convincing benches of evidence that anticipation takes place along the pathway from retina to cortex. This has been observed with a large diversity of recording conditions (in vitro, in vivo, anesthetized, awake), for different animal models (rodent, cat, monkey . . . ). This suggests that there might exist a synergy between the retina, the thalamus-LGN and the cortex to optimize anticipation. This leads to a natural question: How does the dynamical response of the retina to a moving object affect the dynamics changes in the cortex ?

Along these lines, the purpose of this paper is to understand what the retina brings to the primary visual cortex in terms of anticipation, using a computational model, grounded on experimental studies performed at the Institut des Neurosciences de la Timone, in F. Chavane Lab, as well as preexisting models themselves grounded on experiments. Rather than developing a biologically plausible model for one species, the aim of this article is to reconcile two sets of work that have been conducted to model different species, and to study the potential effect of known retinal anticipatory mechanisms on cortical anticipation. The model consists first of a retinal model developed in [3] to confront several potential mechanisms of retinal anticipation (gain control, amacrine cells) and further studied in [9, 10]. This retina model is used as an input to a cortical mean-field model of V1, previously developed by A. Destexhe and his collaborators [11, 12], and calibrated on experimental VSDI signal data on the monkey cortex V1, performed in F. Chavane Lab. Note that, as further discussed in the text, we will not consider the effects of the thalamus (LGN) in this work. More precisely, it will be transparent, considered as a simple relay.

The paper is organized as follows. Section 2 is devoted to methods. We introduce the retino-cortical model in sections 2.1, 2.2 with some complementary elements added in the appendix, section 5.2. In section 2.3 we comment the originality of the model compared to existing work and explain the terminology "Chimera". In section 2.4 we introduce

specific quantities (observables) used throughout the paper to quantify anticipation. Section 3 presents our main results. In section 3.1 we study the VSDI signal response to a moving bar when the retina is passive and brings no anticipatory effect (control conditions). We show that the model qualitatively reproduces the results experimentally observed in [8] with quantitative deviations, presumably due to the lack of anticipation mechanisms coming from the retina. We analyse then the effect of varying the retinal output amplitude (section 3.2.1), the stimulus speed (section 3.2.2), the cortical extent (section 3.2.3), and the conduction speed (section 3.2.4) on cortical anticipation, still in control conditions. We exhibit, at the cortical level, the existence of both anticipation by latency and anticipation by adaptation (peak shift), although the first effect takes over the second in terms of time scales. In section 3.3 we analyse the effect of retinal anticipation mechanisms on cortical anticipation. The section 3.3.1 considers gain control applied either on bipolar cells or retinal ganglion cells on anticipation. Although the main effect of gain control is a strong advancement on the peak shift, it can also modify the retinal ganglion cells response profile, and thereby the cortical response in a nonlinear way, as we show. In section 3.3.3 we analyse the effect of the amacrine cells connectivity on anticipation. Here, we are interested on two types of connectivities. 1) Feed-forward connection from bipolar cells to amacrine cells to retinal ganglion cells, studied e.g. in [2], which specifically suppresses the response to the moving object in the latter half of the receptive field truncating the response and yielding an early response peak. 2), feedback reciprocal connections between bipolar and amacrine cells, both imputing retinal ganglion cells. This generates feedback loops whose main effect is to truncate the bipolar response and yields an advancement of the response peak of bipolar cell [13]. This allows us to compare the respective effects of these two mechanisms on the visual cortex anticipation. In particular, we show that these retina anticipation mechanisms leads to a better quantitative agreement with experimental results. In section 4 we discuss several potential extensions of this work such as more complete models of the retina (including gap junctions or multiple amacrine cells connections), or the inclusion of a mean-field model of the thalamus. The appendix contains additional material concerning the model definition and its parameters.

## 2 Methods

### 2.1 The retina model

This model is made of 3 bidimensional layers whose structure is shown in Fig. 1: A layer of bipolar cells (BCs), a layer of amacrine cells (ACs) and a layer of retinal ganglion cells (RGCs). The layers are rectangle grids, with the same dimension  $L_x \times L_y \text{ mm}^2$  and the same number of cells,  $N$ . BCs are labelled with an index  $i = 1 \dots N$ , ACs are labelled with an index  $j = 1 \dots N$ , RGCs with an index  $k = 1 \dots N$ . Cells are located on the nodes of their grid layer and are spaced by a distance  $\delta \text{ mm}$  in both directions  $x, y$ . Spatial coordinates are noted  $\vec{x} = (x, y)$  and the coordinates of, e.g., BC  $i$  are  $(x_i, y_i)$ .

The 3 layers ought to be parametrised by a vertical coordinate,  $z$ . However, this parametrisation is implicit in the retinal layers label BCs, ACs, RGCs and we are not going to use a vertical distance between layers. Since all layers have the same grid spacing,  $\delta$ , and the same number of neurons, there is a vertical alignment of nodes: the BC with index  $i = 10$  is vertically aligned with the AC of index  $j = 10$  and the RGC with index  $k = 10$ . This given, we define the Euclidean distance between a cells  $i$ , in layer 1, and a cell  $j$ , in layer 2 as  $d(i, j) = \sqrt{(x_i - x_j)^2 + (y_i - y_j)^2}$ . That is, we do not consider the vertical distance, for simplicity. The distance  $d(i, j)$  is used for connectivity patterns.

There is indeed an interlayer connectivity. The connectivity from BCs to ACs is characterized by a connectivity matrix  $\Gamma_A^B$ , with entries  $\Gamma_{A_j}^{B_i} = 1$  if there is a connection from BC  $i$  to AC  $j$ , and  $\Gamma_{A_j}^{B_i} = 0$  otherwise. In the paper, the connectivity structure of  $\Gamma_A^B$  is called "nearest-neighbours+1": the BC with coordinate  $i$  connects to the AC with coordinate  $i$  and with the four nearest neighbours of this AC. The synaptic weight from BC  $i$  to AC  $j$  is then  $W_{A_j}^{B_i} = w_A^B \Gamma_{A_j}^{B_i}$  where the parameter  $w_A^B \geq 0$  controls the excitatory synapses amplitude. This form of synaptic weights allows us to tune the synaptic intensity from BCs to ACs with the unique parameter  $w_A^B$ . The connectivity from ACs to BCs is also characterized by a synaptic weight matrix  $W_B^A$  with entries  $W_{B_i}^{A_j} = w_B^A \Gamma_{B_i}^{A_j}$ ,  $w_B^A \leq 0$  (inhibition from AC  $j$  to BC  $i$ ) where  $\Gamma_B^A$  is "one to one" (AC  $j$  only connects to BC with index  $i = j$ ). The synapse from BC  $i$  to RGC  $k$  corresponds to "Gaussian pooling" [1] where  $W_{G_k}^{B_i} = w_G^B \frac{e^{-\frac{d(i,k)^2}{2\sigma^2}}}{2\pi\sigma^2}$  with  $w_G^B \geq 0$ . Likewise, the connectivity from AC  $j$  to RGC  $k$  is characterized by a synaptic weight  $W_{G_k}^{A_j} = w_G^A \frac{e^{-\frac{d(j,k)^2}{2\sigma^2}}}{2\pi\sigma^2}$  with  $w_G^A \leq 0$ . Synaptic weights are expressed in Hz. The different types of connectivity are summarized in the appendix 5.3.

Cell types have characteristic times, expressed in seconds, corresponding to the integration time of their response to external influence and including synaptic delay. Here, we consider that all BCs have the same characteristic time,  $\tau_B$ . Likewise, all ACs have a characteristic time,  $\tau_A$ , and RGCs a characteristic time,  $\tau_G$ .

The dynamics of cells is based on their voltage. We note  $V_{B_i}$ , the voltage of BC  $i$  and so on. Voltage rectification takes place below a certain threshold (eq. (3)). In addition, BCs and RGCs have gain control, a desensitization when activated by a steady illumination. (eq. (5), (8)), characterized by an activation variable  $A_{B_i}$  for BCs,  $A_{G_k}$  for RGCs [14]. The dynamics of voltages and activations is given by eq. (2) below.

BCs receive a visual input featuring the pre-processing of a visual stimulus via photo-receptors and horizontal cells. In this study, a visual stimulus is a grey scale video, that is a function  $\mathcal{S}(\vec{x}, t) \in [0, 1]$  where 0 corresponds to black and 1 to white. The pre-processing of this visual stimulus via photo-receptors and horizontal cells is modelled by a spatio-temporal convolution:

$$\left[ \mathcal{K}_{B_i} \overset{\vec{x}, t}{*} \mathcal{S} \right] (t) \equiv V_{i_{drive}}(t), \quad (1)$$

where  $\mathcal{K}_{B_i}(\vec{x}, t)$  is a spatio-temporal kernel, centered at the coordinate of the BC  $i$ , and called "OPL kernel" (where "OPL" stands for "Outer Plexiform Layer" <https://www.ncbi.nlm.nih.gov/books/NBK11518/>). Spatially, this is a Gaussian with a center of radius  $\sigma_c$  and temporally, a gamma function with a characteristic time  $\tau_c$  (see appendix 5.1 for the value of these parameters). Therefore, the OPL input of BCs is monophasic in space and time. As shown in [10] the presence of lateral inhibition (here, by ACs) allows nevertheless to generate biphasic profiles in space and in time for the BCs response. Note that the spatial RF is circular: we do not consider orientation selective cells in this paper. In the definition of  $\mathcal{K}_{B_i}$  there is a multiplicative factor,  $\mathcal{C}$ , which allows us to control the amplitude of  $V_{i_{drive}}(t)$ . This is used, in section 3.2.1, to modify the amplitude of the retinal input to the cortex.

The joint evolution of BCs, ACs, RGCs, driven by the stimulus  $\mathcal{S}$  is given by the following set of equations. We use the standard notations of dynamical systems theory, where the time variable is omitted except for the non autonomous term (here, the drive term). We refer to the papers [3, 9, 10] for detail about this model.

$$\left\{ \begin{array}{l} \frac{dV_{B_i}}{dt} = -\frac{V_{B_i}}{\tau_B} + \sum_{j=1}^{N_A} W_{B_i}^{A_j} V_{A_j} + V_{i_{drive}}(t), \\ \frac{dA_{B_i}}{dt} = -\frac{A_{B_i}}{\tau_{\alpha_B}} + h_B \mathcal{N}_B(V_{B_i}), \\ \frac{dV_{A_j}}{dt} = -\frac{V_{A_j}}{\tau_A} + \sum_{i=1}^{N_B} W_{A_j}^{B_i} R_B(V_{B_i}, A_{B_i}), \\ \frac{dV_{G_k}}{dt} = -\frac{V_{G_k}}{\tau_G} + \sum_{j=1}^{N_A} W_{G_k}^{A_j} V_{A_j} + \sum_{i=1}^{N_B} W_{G_k}^{B_i} R_B(V_{B_i}, A_{B_i}), \\ \frac{dA_{G_k}}{dt} = -\frac{A_{G_k}}{\tau_{\alpha_G}} + h_G \mathcal{N}_G(V_{G_k}), \end{array} \right. \quad (2)$$

where, in addition to voltages, we have introduced the activity variables,  $A_{B_i}$  for BCs,  $A_{G_k}$  for RGCs, ruling the gain control mechanisms on these cell type. There is no gain control on ACs. BCs are, in addition, rectified. The function:

$$\mathcal{N}_B(V_{B_i}) = \begin{cases} 0, & \text{if } V_{B_i} \leq \theta_B; \\ V_{B_i} - \theta_B, & \text{else,} \end{cases} \quad (3)$$

models this BCs voltage rectification, where  $\theta_B$  is the rectification threshold. The BCs output to ACs and RGCs is then characterized by a non linear response to its voltage variation, given by :

$$R_B(V_{B_i}, A_{B_i}) = \mathcal{N}_B(V_{B_i}) \mathcal{G}_B(A_{B_i}), \quad (4)$$

where the function:

$$\mathcal{G}_B(A) = \begin{cases} 0, & \text{if } A \leq 0; \\ \frac{1}{1+A^6}, & \text{otherwise.} \end{cases} \quad (5)$$

implements the gain control of BCs as a function the activity variable  $A_{B_i}$  [1].

As ganglion cells are spiking cells, their response function is:

$$R_G(V_{G_k}, A_{G_k}) = \mathcal{N}_G(V_{G_k}) \mathcal{G}_G(A_{G_k}). \quad (6)$$

This function corresponds to a probability of firing within a small time interval. Thus, it is expressed in Hz. Consequently,  $\alpha_G$  is expressed in Hz  $\text{mV}^{-1}$  and  $N_G^{max}$  in Hz. A non-linearity is fixed so as to impose an upper limit over the firing rate. Here, it is modeled by a piece-wise linear function :

$$\mathcal{N}_G(V) = \begin{cases} 0, & \text{if } V \leq 0; \\ \alpha_G(V - \theta_G), & \text{if } \theta_G \leq V \leq N_G^{max}/\alpha_G + \theta_G; \\ N_G^{max}, & \text{else.} \end{cases} \quad (7)$$

We have, for the RGCs gain control:

$$\mathcal{G}_G(A) = \begin{cases} 0, & \text{if } A \leq 0; \\ \frac{1}{1+A}, & \text{else.} \end{cases} \quad (8)$$

which actually differs from the non-linearity in the BCs gain control, following [14]. The gain control rate,  $h_B$  for BCs,  $h_G$  for RGCs, expressed in Hz  $\text{mV}^{-1}$ , tunes the intensity of the gain control. In particular, if  $h_B = 0$ ,  $A_{B_i} \rightarrow 0$  exponentially fast so that the gain  $\mathcal{G}_B(A) = 1$ . The same remark holds for RGCs.

Parameters values of the model can be found in the appendix 5.1.

## 2.2 The cortical model

This is a two dimensional model composed of two populations of cortical columns: excitatory (E) and inhibitory (I), located in a cortical area of dimension  $\alpha L_x \times \alpha L_y$ , where  $\alpha$  is a magnification factor from retina to cortex. Cortical columns represent the spatial average of cortical neurons at a space scale roughly corresponding to one pixel of voltage sensitive dye imaging (VSDI signal) [15]. This model has actually been employed in [16] to reproduce the VSDI response to a simple visual stimuli (apparent motion) in the awake monkey primary visual cortex (V1). Cortical spatial coordinates are noted  $(x, y) \equiv \vec{x}$ . We thus use the same notations as for the retina, to alleviate notations, although there is a magnification factor between these two systems of coordinates.

The activity of cortical columns is represented by their average firing rate:  $\nu_E$  for excitatory columns,  $\nu_I$  for inhibitory columns. The equations for cortical neurons dynamics are based on a mean-field model of Adapting Exponential (AdEx) neurons [17]. This model was derived under the hypothesis that the network dynamics is Markovian at a timescale of a few ms and stationary for a duration  $T$ . One describes then the collective dynamics through a master equation formalism developed by El Boustani and Destexhe [18]. This system can reproduce asynchronous irregular regime, a typical feature of the awake states, as well as Up and Down states, characteristic of sleep or anesthesia states [17].

The spatially extended dynamical system reads:

$$\begin{cases} T \frac{\partial \nu_E(\vec{x}, t)}{\partial t} = -\nu_E(\vec{x}, t) + F_E \left[ \nu^{aff}(\vec{x}, t) + \nu^{drive} + A_E^E \nu_E^{input}(\vec{x}, t), A_E^I \nu_I^{input}(\vec{x}, t) \right] \\ T \frac{\partial \nu_I(\vec{x}, t)}{\partial t} = -\nu_I(\vec{x}, t) + F_I \left[ \nu^{aff}(\vec{x}, t) + \nu^{drive} + A_I^E \nu_E^{input}(\vec{x}, t), A_I^I \nu_I^{input}(\vec{x}, t) \right], \end{cases} \quad (9)$$

where  $\nu_E(\vec{x}, t)$  (resp.  $\nu_I(\vec{x}, t)$ ) is the population rate of the excitatory (resp. inhibitory) cortical column located at  $\vec{x}$ , at time  $t$ .  $T$  is the characteristic integration time.

In eq. (9) the functions  $F_E$  (resp.  $F_I$ ) are the transfer functions of excitatory (resp. inhibitory) neurons. They describe the firing rate of population  $E$  (resp.  $I$ ) as a function of the excitatory and inhibitory rates  $\nu_E$  and  $\nu_I$ . Their form is made explicit in the appendix, section 5.2. The term  $\nu^{aff}(\vec{x}, t)$  in eq. (9) corresponds to the retino-thalamic input (sensory drive). As the thalamus is not considered here (we assimilate it to a simple relay) this input comes directly from the RGCs. There is a direct correspondence, a retinotopy, between a point in the retina (RGC), and a point in V1 (cortical column). Here, this mapping is linear. There is just a magnification factor  $\alpha$  from the retina to V1. Each RGC inputs a cortical column and  $\nu^{aff}(\vec{x}, t)$  is the firing rate emitted by the RGC that inputs the cortical column located at  $\vec{x}$ . Note that, in the absence of gain control or amacrine connectivity, the retinal model is reduced to a convolution cascade [3, 9, 10]. In this case, the input  $\nu^{aff}(\vec{x}, t)$  is therefore similar to the one used in [8]. In the transfer functions  $F_E, F_I$ , we include a spatially uniform external drive  $\nu^{drive}$ . This drive represents the background constant input coming from the rest of the brain.

$\nu_E^{input}(\vec{x}, t)$  (resp.  $\nu_I^{input}(\vec{x}, t)$ ) are excitatory (resp. inhibitory) inputs coming from the column itself or from other cortical columns. They are multiplied by an amplification connectivity factor  $A_{post}^{pre}$ , where  $pre$  and  $post \in E, I$  stands respectively for "pre synaptic" and "post synaptic". In our case  $A_E^E = A_I^I = A_E^I = 1$  and  $A_I^E = 1.5$ . This connectivity corresponds to the observed physiology of the real cortex. We have:

$$\begin{cases} \nu_E^{input}(\vec{x}, t) = \int_{\mathbb{R}^2} \mathcal{N}_E(\vec{x} - \vec{x}') \nu_E(\vec{x}', t - \|\vec{x}' - \vec{x}\|/v_c) d\vec{x}' \\ \nu_I^{input}(\vec{x}, t) = \int_{\mathbb{R}^2} \mathcal{N}_I(\vec{x} - \vec{x}') \nu_I(\vec{x}', t - \|\vec{x}' - \vec{x}\|/v_c) d\vec{x}' \end{cases} \quad (10)$$

where  $\mathcal{N}_E, \mathcal{N}_I$  are 2D circular Gaussian connectivity kernels with mean-square deviation  $\sigma_E, \sigma_I$ :

$$\mathcal{N}_X(\vec{x}) = \frac{e^{-\frac{1}{2} \frac{\|\vec{x}\|^2}{\sigma_X^2}}}{2\pi\sigma_X^2}, \quad (11)$$

with  $X = E, I$ . This form follows e.g. [11], although our connectivity kernel is two dimensional in contrast to their paper. Thus,  $\sigma_E, \sigma_I$  control the two dimensional cortical extent of the excitatory and inhibitory connections. Note, that, due to the normalisation of the Gaussian the shorter the cortical extent the larger the amplitude of the synaptic weight  $\mathcal{N}_X(\vec{x})$  (see section 3.2.3 for a consequence of this). The parameter  $v_c$  is the speed of axonal conduction (assumed to be a constant). Equations (10) therefore express that the excitatory input  $\nu_E^{input}(\vec{x}, t)$  is the sum of the incoming excitatory activity from the connected columns arising with a delay  $\|\vec{x}' - \vec{x}\|/v_c$  depending on the distance between the columns and the axonal conduction speed.

The cortical model is designed to reproduce the pixels intensity of voltage sensitive dye imaging, corresponding to a variation of fluorescent luminosity with respect of the fluorescent baseline. Its expression depends on the average membrane potential of the excitatory and inhibitory populations in the column located at  $\vec{x}$ , at time  $t$ . Its expression is given by equation (22) in the appendix, section 5.2.

**Remark.** Note that this type of cortical model can exhibit pathological (i.e. model induced) oscillations due to bifurcations when some parameters become too large (such as  $\nu^{drive}$  or the conduction speed). This phenomenon is well known and has been reported in the literature [19]. We observe as well such oscillations when parameters such as the retinal output amplitude becomes too large. This is commented in the afferent section.

### 2.3 Specific features of the model

In addition to propose an original implementation of the retino-cortical V1 system, the model has specific features. First, this is a two dimensional model in space, allowing to play complex trajectories and actually, to simulate the response to realistic visual scenes. This is a feature of the simulator we use, called Macular, developed at Inria. Macular is a simulation platform for the retina and the primary visual cortex (V1), designed to reproduce the response to visual stimuli, in normal vision conditions, or in altered conditions (pharmacology, pathology, development). It is organised into a layered structure that mimics the multi-layers organisation of the retina. It is fed by visual inputs (movies) then processed by the multi-layer structure. A description can be found at [https://macular.gitlabpages.inria.fr/macular/user\\_doc/Macular/main.html](https://macular.gitlabpages.inria.fr/macular/user_doc/Macular/main.html).

In contrast to previous models which were considering retino-thalamic entries as spatially periodic functions (rings), the mere fact of introducing realistic retinal inputs leads to a distinction between left and right, bottom and top so that one cannot consider rings geometries anymore. In contrast, we need to define proper boundary conditions to the model. Here, we assume zero boundaries conditions for the retinal and the cortical model. In contrast to ring topologies, this induces spatial inhomogeneities, even when considering the rest state.

Finally, this model is a "chimera" model in the following sense. While the design and parameters of the cortical model are based on previous works on the monkey visual cortex, the retinal model is essentially based on previous works dealing with mice retinas. In addition, as mentioned above, there is no thalamus, or, more precisely, it is transparent, considered as a simple relay. In this sense, our model resembles more a "Frankenstein" creature than a real, actual organism. However, we believe that it captures the main mechanisms in the retino-cortical entanglement. Also, the advantage of such a model, with its joint simulation platform, is that one can easily modify the parameters of such or such components and see how it modifies the observed response. This is actually the main philosophy of this work where we vary physiological parameters, such as the conduction speed, or the effect of amacrine cells, that cannot be easily varied experimentally. This also means that the chimera model could be made closer to monkeys by adjusting the retina model to experimental results on monkeys retinas. Note that a feature of the simulator Macular is precisely to afford such changes.

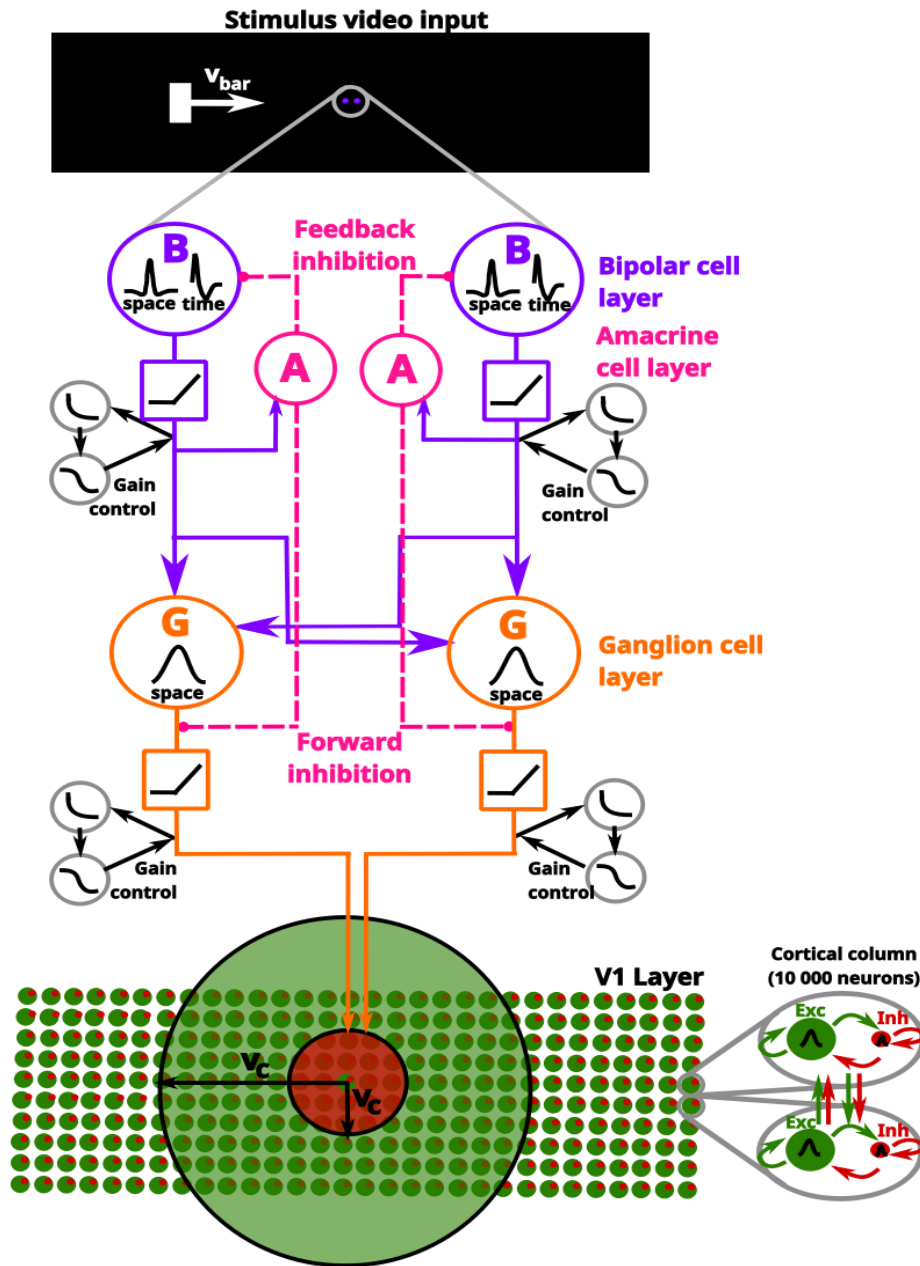


Figure 1: **Synthetic view of the retino-cortical model.** A stimulus is perceived by the retina, triggering a response. **From top to bottom:** The stimulus is first convolved with a spatio-temporal receptive field (black traces labelled "space" and "time" in the purple circles), that mimics in the Outer Plexiform Layer (OPL) the concerted activity of photoreceptors and Horizontal cells and is fed to Bipolar cells (purple circles). This response is rectified by a low voltage threshold (purple squares). Bipolar cells responses are then pooled to retinal Ganglion cells (orange). The firing rate response of a Ganglion cell is a sigmoidal function of the voltage (orange square). Gain control can be applied at the Bipolar and Ganglion cells level (grey circles) triggering anticipation by a shift in the time to peak. The Bipolar cells activity is modulated by lateral inhibition through Amacrine cells (pink). The Ganglion cells response (firing rate) is sent to cortical columns in the primary visual cortex depicted, at the bottom right, as two interconnected mean field units (small circles) corresponding respectively to excitatory (green) and inhibitory (red) population. A sketch of this interconnection is shown on the right zoom (grey circles). Cortical columns are connected together by an excitatory (big green circle) and inhibitory (big red circle) lateral connectivity. Note that we assume the same conduction velocity  $v_c$  for both connectivities.



## 2.4 Observables for anticipation

From now, both simulated retinal and cortical areas are 2D spaces of  $81 \times 15$  retinal cells. As two consecutive retinal or cortical columns are spaced by  $0.225^\circ$  of visual angle these areas correspond to  $18.225^\circ \times 3.375^\circ$ . Using the conversion factor of about 0.3 mm per degree in the retina, approximated from <https://www.ncbi.nlm.nih.gov/books/NBK11556/> and 3 mm per degree in the cortex for humans this gives a retinal area of  $\sim 5.46 \times 1 \text{ mm}^2$  and a cortical area of  $54.6 \times 10 \text{ mm}^2$  with a spacing of  $67.5 \mu\text{m}$  between retinal cells and  $675 \mu\text{m}$  between cortical columns. We discard the first and the last horizontal degree in all figures to reduce boundaries effects, giving thus an effective cortical space of  $16.45^\circ$  long.

In this paper, we mainly consider the motion of a bar, moving horizontally, from left to right, along the  $x$  axis with a constant speed  $v_B$ . The bar starts to move at time  $t = 0$  where the center of the RF of the cortical column located at  $x = 0$  coincides with the middle of the bar. The bar has dimensions  $0.67 \times 0.9$  degrees of visual angle, i.e. its height is small compared to the vertical extent of the retina and the cortex. As a consequence, we will consider, in the definition of anticipation observables, that the bar response is characterized by two dimensional graphs, with one spatial dimension,  $x$ , and the time,  $t$ .

### 2.4.1 Cortical anticipation

In this section, we define several observables related to the cortical activity when responding to the moving bar. These observables are here introduced in a case where the sensory drive of the cortical model consists of the retinal response to a white bar with neither gain control nor amacrine cells. This especially means that the retina is passive. We refer this as control conditions (CTL). All parameters are given in the table 1 of the appendix. The illustrative figure 2 corresponds to a bar moving at  $6^\circ/s$  (equivalent to 18 mm/s in the cortex). This is also the value of the default bar speed.

The indicators for cortical anticipation are based on the typical VSDI signal curves, shown in Fig. 2A, and reproducing the experimental observations made by [8]. We first define quantities attached to individual columns, i.e. depending on the spatial coordinate  $x$ .

#### Local observables.

- $t_{center}(x)$  is the time when the middle of the bar reaches the center of the receptive field of the column located at  $x$ . We have  $t_{center}(0) = 0$ .
- **The activation time (AT)**,  $t_{ON}(x)$ , is the time when the VSDI signal response becomes larger than a threshold  $\theta = 0.001$ .
- **The latency** is  $t_L(x) = t_{ON}(x) - t_{center}(x)$ . Since  $t_{ON}(x) \leq t_{center}(x)$ , the latency can be negative or equal to 0. The latency increases therefore when its value become more negative.
- **The time to peak (TTP)** is the time  $t_P(x)$  when the VSDI signal has its maximum (see Fig. 2B).
- **The peak delay** is  $t_{PD}(x) = t_P(x) - t_{center}(x)$ . This quantity can, a priori, have any sign, although in CTL conditions it is always positive. This value can be negative though due to e.g. to the retina influence.

The latency,  $t_L(x)$ , depends on the distance of the column to the point where the bar started. To illustrate this dependence we use a color code, similarly to the paper [8]. The different cortical columns positions in the V1 field are represented by a color gradient (see Fig. 2B), from black ( $x = 0$  degree, point where the bar starts) to light blue ( $x = 18.45$  degree). Although, for a spatio-temporal representation  $x, t$ , there is a redundancy between the  $x$  coordinate and the color, this representation is actually quite didactic and insightful. Especially, as shown in Fig. 2B, if one shifts all these curves so that their peak coincides, one observes a change in the shape of the response prior to the peak: the latency increases with the distance to the bar origin, so that the columns start to respond earlier and earlier. Following [8] we interpret this as a *cortical anticipation by latency*. We now introduce global observables to quantify this form of anticipation.

**Global spatial observables.** Although the latency corresponds to a time as a function of space, it is useful to invert the axes and, instead, to represent space as a function of time: the curve  $t_L(x)$  becomes  $x(t_L)$  by a simple symmetry with respect to the first diagonal. The cortical space, plotted in function of the activation time and the time to peak have characteristic shapes illustrated in Fig. 2C. This allows us to define four spatial observable, following Benvenuti et al [8]:

- **The anticipation range (AR)** is the maximal spatial limit of anticipation, the maximal distance at which cortical columns constructively interact to anticipate motion, as argued in [8]. It corresponds to the ordinate of the inflexion point in Fig. 2C. Beyond this spatial position, anticipation saturates because lateral connectivity,

which causes anticipation, has a finite radius. Consequently, beyond the anticipation range, the slope of the activation time becomes constant (Fig. 2C), the activation time is no longer affected by the lateral cortical propagation, but only by the bar speed.

- **The short-range activation speed (SRAS)** is the slope of the activation time before the inflection point (Fig. 2C). This speed, actually sums up two different contributions: the bar speed and the anticipation speed carried by lateral connectivity (Fig. 2C).
- **The Long range activation speed (LRAS)** is the slope of the activation time after the inflection point. This cortical region is characterized by an absence of lateral cortical connectivity influence. In our model, its slope is only constrained by the bar speed. We mention this quantity because it is expected to vary due to feedback effects [8] and would become relevant with a model including a thalamus-LGN (see discussion).
- **The Peak speed (PS)** is the slope of the time to peak curve. It is parallel to the moving bar curve. It is constant in our case, because the bar speed is constant.

**Global temporal observables.** One can also plot  $x$  as a function of the latency (see figure 2D). We obtain two temporal observables, illustrated in Fig. 2D:

- **The maximal latency (ML).** One observes that the latency of cortical columns close from the starting point of the bar (black circles) increases until saturation as the columns are located further and further from the starting point of the bar. The saturation value is the maximal latency.
- **The standard peak delay (SPD).** In contrast to ML, the peak delay is actually independent of  $x$ , in all the cases studied in the paper. We discuss this homogeneity in the discussion section. We call this value the SPD.

**Interpretation.** The figure 2 essentially shows that the moving bar triggers a wave of cortical activity, transmitted by the columns sensing the bar to the distant columns via the lateral connectivity, at a speed which accumulates the bar speed and the axonal velocity (Fig. 2B and C). This reproduces the observations of Benvenuti et al. [8] and was interpreted by the authors as an indication that cortical anticipation mainly holds by latency. The accumulation of the signals sent by the columns sensing the bar, via the lateral connectivity, advances the time when the distant columns - not yet sensing the bar - start nevertheless to respond to it. This is the explanation of the change in the early VSDI response profile (before the peak), in Fig. 2B, as a function of the color gradient. One observes therefore that the latency becomes more and more negative with the distance of the cortical column to the position where the bar starts, Fig. 2D, meaning that the cortical columns are informed earlier and earlier that something is arriving. This observation holds until a saturation value, the maximal latency, where the gain of anticipation provided by the lateral cortical connectivity reaches a maximum. This suggests that cortical connectivity and axonal velocity impacts anticipation (sections 3.2.3, 3.2.4). As developed below, we also observe an anticipation by peak shift, where the peak in the VSDI signal is advanced with respect to the peak in the RGCs response.

## 2.4.2 Retinal anticipation

Anticipation has also been observed in the retina, according to different modalities. The first characterization was provided Berry et al. [1]. It is characterized by a shift in the peak of the ganglion cell response to a moving object, occurring before the peak response to the same object when flashed [1, 14]. This can be explained by gain control which has the effect of advancing the peak response of the cell's activity. In our model, this effect can arise at the level of BCs or RGCs. A detailed study was published in [3]. It shows that, with gain control, anticipation time grows with the size and the contrast of the bar while it decreases with its velocity. In our retina model, amacrine cells can also induce anticipation by advancement of the peak, independently of gain control, although these two effects can constructively combine. We qualify this peak shift mechanism as *peak anticipation* or *adapting anticipation* (using the terminology of [2]) since BCs and RGCs adapt according to their level of activity. Therefore, we quantify retinal anticipation by a RGC peak shift and we define the same peak-based quantities as for the cortical case (time to peak and SPD).

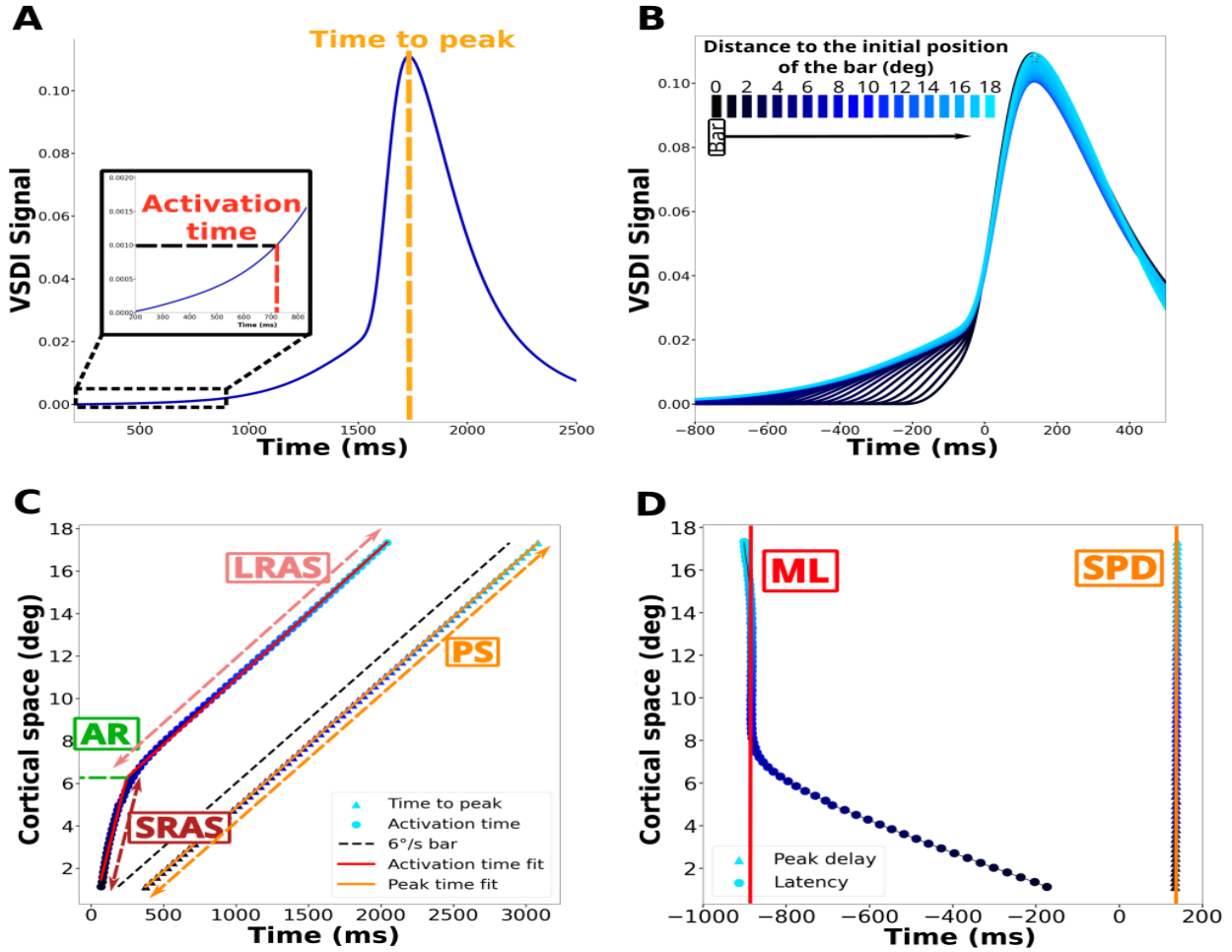


Figure 2: **The paradigm of cortical anticipation by latency.** **A)** Typical time course of the VSDI signal response for a fixed cortical column located at  $x$ . The time to peak corresponds to the yellow dotted line. The insert shows a zoom of the proximal part of the curve where the activation time is computed (the black dotted line corresponds to the threshold  $\theta$ , see text.). **B)** Global representation of the spatio-temporal VSDI responses using a collapse of the VSDI signals. The curves corresponding to cortical columns located at different spatial locations are shifted so that their maximum coincides. Then, these curves are colored so that the different cortical columns positions in the V1 field are represented by a color gradient (displayed on the top of the figure), from black ( $x = 0$  degree, point where the bar starts) to light blue ( $x = 18.45$  degree). The legend at the top left represents the color gradient (from black to light blue) associated with the position of the cortical column. **C)** inverted time space representation where the cortical space ( $x$  coordinate, in degrees of visual angle) is represented as a function of time (in ms). The dotted black line corresponds to the displacement of the center of the moving bar. This is a straight line,  $x = v_B t$  (the center of the bar is located at  $x = 0$  when  $t = 0$ ). The time to peak,  $t_P(x)$ , is represented by triangles, colored according to the color gradient. The curve (orange line) is a straight line too, with equation  $x = v_B (t - t_P(0))$ , where  $t_P(0)$  is the time to peak for the column located at  $x = 0$ . The peak speed (PS) is the slope of this curve (thus, in CTL conditions, this is the bar speed,  $v_B$ ). The activation time,  $t_{ON}(x)$  is represented by circles colored according to the color gradient. The curve represents a crossover between two regimes, well fitted by straight lines (red curves), and separated by an inflection point. The spatial position of this inflection point is the anticipation range (AR). The slope of the first linear part (dark red dashed arrow) corresponds to the short-range activation speed (SRAS). The slope of the second linear part (light red dashed arrow) is the long range activation speed (LRAS). In CTL conditions, this slope is equal to  $v_B$ . **D)** Maximal latency (ML) and Standard Peak Delay (SPD). The cortical space is represented as a function of the latency (in ms). The latency increases until saturation (red vertical line), at a time called maximal latency (ML). The peak delay (triangle) is constant and equal to the standard peak delay (SPD), (yellow vertical line).

### 3 Results

#### 3.1 Model calibration

The model was calibrated so as to reproduce the results obtained by [8] in the monkey primary visual cortex. Note however that, although our color gradient is similar to the one used by these authors, it corresponds to different positions. Indeed, in our simulations, the cortical area used is bigger than in their experiments (18 degrees versus 7 degrees). A larger simulated cortical area was indeed needed to be able to correctly observe the effect of certain parameters such as bar speed or cortical latency.

The figure 2 illustrates the result of our model in CTL conditions, with a bar speed of  $6^\circ/s$ . Our model reproduces the shape of the latency curve shown in [8], Fig. 4: cortical columns far from the bar origin are activated much earlier than the ones close to the bar origin. This curve is divided in two regimes, reproduced by our model, commented in section 2.4 and illustrated in Fig. 2. In the first regime (short-range activation) the slope have a value of  $24.8^\circ/s$  in experimental data and of  $21.3^\circ/s$  in simulated data. The inflection point differs though:  $2^\circ$  in experiments and  $6.3^\circ$  in simulations. Also, the activation in our model can occur up to 880 ms before the center of the bar arrives at the center of the receptive field (i.e. a maximal latency of  $-880$  ms) while in [8] it is said that "latency scatter for the medium and long trajectories that fully covered a wide range of values from 0 to  $-400$  and  $-800$  ms". We finally note a difference in the time of the peak, very close to zero in experiments (Fig. 4D of [8]) but located at 139 ms in the simulation. To understand these discrepancies, it is important to note that our simulations are made in control conditions i.e. without any retinal anticipation mechanism, whereas such mechanisms are presumably present in experimental conditions. Indeed, as commented later, adding retinal anticipation reduces these differences (section 3.3). Taken together, these results provide a good basis for further explorations on the role of retinal and cortical effects on anticipation with discrepancies expected to be reduced in the presence of a realistic retinal input.

#### 3.2 Cortical anticipation depends on stimulus features and on physiological parameters

We now study study, in CTL conditions, the dependence of anticipation on several parameters, such as the bar speed or contrast, and physiological parameters, such as the conduction speed following the modalities described in section 3.2. The default value of the parameters, including the bar speed, are those reported in the Appendix 5.1.

##### 3.2.1 Increasing the retinal output amplitude enhances anticipation

We varied the retinal output amplitude (ROA), sent by retinal ganglion cells, in a range from 1 to 50 Hz (figure 3). For this, we increased the amplitude  $C$  of the OPL kernel (eq. (1)). This has the effect of increasing the firing rate of the RGCs in a linear way. Note that we are still in CTL conditions here, the retina is passive. Increasing the retinal input increases almost linearly the VSDI signal (Fig. 3 E) with a slight saturation presumably due to the sigmoid activation functions  $F_E, F_I$  in the mean field model of cortical columns (eq. (9)). Here, we chose to stay in the almost linear range. Indeed, we observed that increasing too much the amplitude of the input leads to pathological oscillations which, as mentioned above, are artefacts of the cortical model.

The collapse of VSDI signals, shown in Fig. 3 A (1 Hz) and Fig. 3 B (35 Hz), has globally the same shape as the paradigmatic figure 2A, although we observe a clear difference in the latencies between A and B. This is a first indication that increasing the ROA enhances anticipation by latency. Fig. 3 C shows the temporal profile of the VSDI signal for the cortical column located at the center of the lattice ( $x = 9^\circ, y = 1.35^\circ$ ). One observes an increase in the slope before the peak, resulting in an increase of the maximal latency (ML) which becomes more negative as shown in Fig. 3 F (red trace). There is a saturation for large retinal inputs amplitude though. Along the same lines, we plot, in 3 D, the spatial VSDI signal for the time when the central cortical column reaches its maximum. Note that the  $x$  coordinates has been shifted so that the central cortical column is actually located at  $x = 0$  in this figure. We observe a spread of the left part of the peak and a more abrupt slope on the right part, as the ROA increases. Those combined effects results in a increase of the anticipation range (AR) as shown in Fig. 3 F (green trace), with again a saturation effect. Finally, the spatial and temporal effects combine to increase the short range anticipation speed (SRAS). Therefore, anticipation by latency becomes more prominent (ML and AR) and spreads faster (SRAS) as the ROA increases.

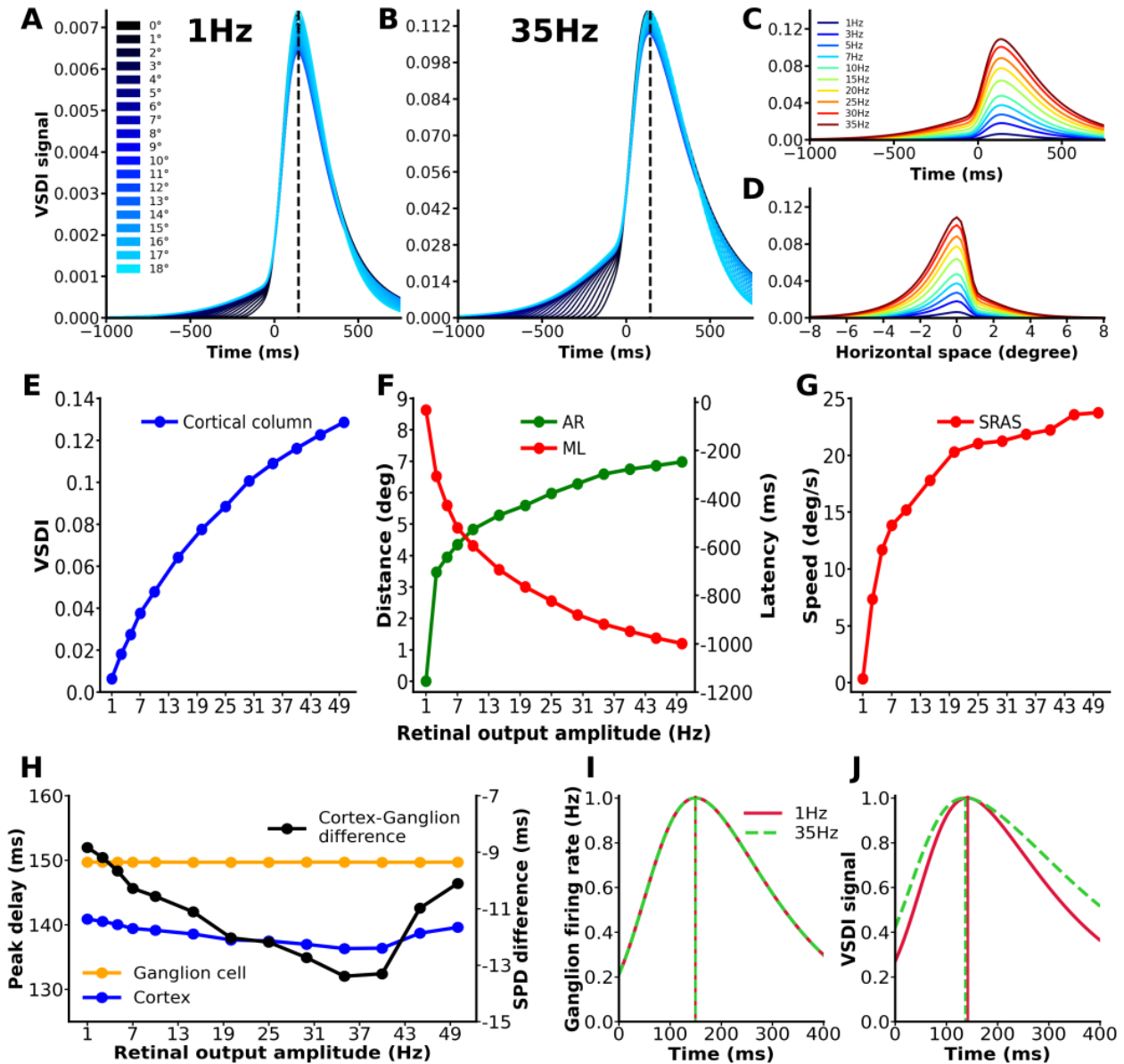


Figure 3: **The effect of the retinal output amplitude (ROA) on the cortical response.** VSDI signal response to ROA at **A**, 1 Hz and **B**) 35 Hz. The color bar on the left of Fig. A represents the color gradient introduced in section 2.4. **C**) **Temporal VSDI signal** in response to increasing retinal amplitude for the cortical column located at the center of the lattice ( $x = 9^\circ, y = 1.35^\circ$ ). **D**) **Spatial VSDI signal** in response to increasing retinal amplitude, for the time where the central cortical column reaches its maximum. The  $x$  coordinates has been shifted so that the central cortical column is actually located at  $x = 0$ . **E**) **VSDI signal amplitude** of the central cortical column versus the ROA. **F**) **Temporal and spatial observables**: maximal latency (red, scale on the right) and anticipation range (green, scale on the left) versus the ROA. **G**) **Speed observable**: short-range activation speed (red) versus the ROA. **H**) **Retino-cortical SPD variation** versus the ROA for the central cell. The ganglion firing rate SPD is plotted in orange and the VSDI signal in blue (scale on the left). In black, is represented the difference between the cortical and RGC SPD (scale on the right). A negative value means a cortical peak arising earlier than the RGC peak. **I**) **Shape of the central RGC response profile to the moving bar**, for 1 Hz (red) and 35 Hz (dashed green). Note that the red trace is normally quite smaller than the green trace, but we have rescaled it to show that the difference between 1 Hz and 35 Hz, at the retinal input level, is only a rescaling. This contrasts with **J**) **VSDI signal**, where the same rescaling let also appear distortions due to the non linearities in the cortical model. The dotted vertical lines in I, J correspond to the peaks in the RGCs firing rate or VSDI signal at 1 Hz (red) and 35 Hz (green).

Interestingly, we also observe a slight anticipation by peak shift. This appears in Fig. 3 C where we remark a shift of the time to peak as the ROA increases. For a more quantitative study we have plotted in Fig. 3 H the SPD as a function of the ROA. It is constant for RGCs, but essentially decreases for the cortex. This figure also shows the difference between the cortical and retinal SPD, which is negative, meaning that the VSDI peak arises earlier than the RGC frequency peak. Thus, in addition to show anticipation by latency, the VSDI signal is also a bit in advance on the RGC peak. This effect is primary due to the cortical lateral connectivity. It decreases when the cortical extent decreases as further commented in section 3.2.3. It is enhanced when the retinal input increases, up to some maximum at about 35 Hz, where the difference is maximal, i.e. where the VSDI peak anticipates the most the RGC frequency peak. However, beyond 35 Hz, we start to observe (small) oscillations in the VSDI signal so that the increase of the curve after 35 Hz might be an artefact of the model. It is interesting to note that even at small retinal amplitudes (1Hz), the cortex remains 8.8 ms ahead of the retina. In Fig. 3 I we have plotted the time profile of the frequency response near the peak for the central RGC, and, in Fig. 3 J, the time profile of the VSDI, near the peak for the central cortical column. The red traces correspond to a 1 Hz ROA and the green traces to 35 Hz. The green traces have actually been rescaled to match the amplitude of the red ones. This is to show that, in addition to a simple rescaling (which makes the RGC response overlap in Fig. 3 I), there are, in the cortex, non linear effects which modify the shape of the response and thereby impact the anticipation.

To summarize, an increase in the ROA non-linearly enhances the anticipation which extends further, earlier and faster, with a saturation when the amplitude of the retinal input becomes too large. Rising the ROA increases the overall activity level transmitted laterally by cortical columns. Thus, more distant cortical columns are above the threshold earlier as shown by the increase in ML and AR. The results also demonstrate the presence of a mechanism in the cortex enabling anticipation by peak shift, an effect which increases with the amplitude of retinal input. This effect is quite weaker though than the anticipation by latency (maximum 15 ms for the peak delay and minimum 200 ms for the latency).

**Stimulus contrast.** We assessed the impact of the stimulus contrast in the movies by increasing it from 0.1 to 1 by increments of 0.1. As we checked (Fig. 4) the effect is completely equivalent to increasing the amplitude  $C$  of the OPL kernel and thus, the amplitude of the retinal input.

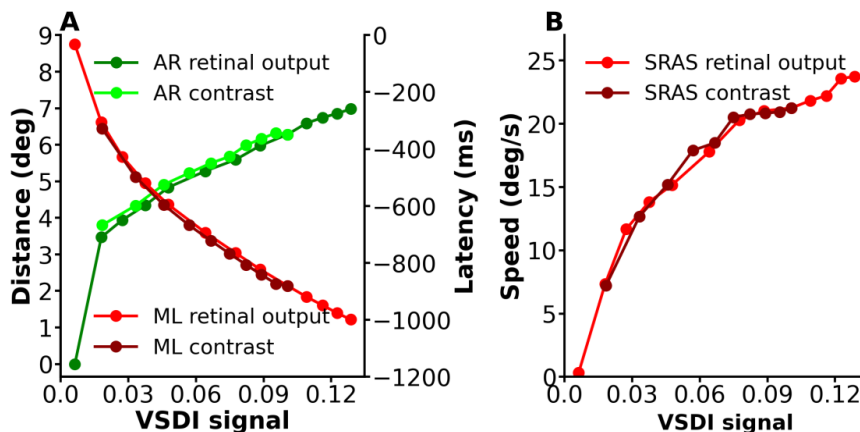


Figure 4: **Stimulus contrast and retinal output amplitude comparison.** **A) Temporal and spatial observables in function of VSDI amplitude:** Maximal latency with retinal output (red) or stimulus contrast (dark red) variant. Anticipation range with retinal output (green) or stimulus contrast (light green) variant. **B) Speed observable:** short-range activation speed with retinal output (red) or stimulus contrast (dark red) variant.

### 3.2.2 Cortical anticipation non monotonously depend on the bar speed

We have done simulations with speeds ranging from  $3^\circ/s$  (equivalent to 18 mm/s of the cortex) to  $30^\circ/s$  (resp. 90 mm/s in the cortex), still in conditions where the retina is passive, with the default parameters of Appendix 5.1. Our results are summarized in Fig. 5. The first remark is that, increasing the bar speed decreases the amplitude of the retinal input. This is because the OPL kernel  $\mathcal{K}_{B_i}$  in eq. (1) has less time to integrate the stimulus. We actually see the decrease in the BCs activity and RGCs activity as the bar speed increases (Fig. 5 A). This induces a decrease in the VSDI signal activity (Fig. 5 B). Thus, from the conclusions of the previous section, one expects a reduction of the anticipation by latency. Increasing the bar speed indeed diminishes the ML and the AR (Fig. 5C).

Is this effect on ML and AR only due to the ROA reduction or are there more subtle, non linear, effects hidden ? To address this question we plotted ML, AR as a function of the ROA itself controlled by the bar speed and compared to the case of Fig. 3 F where the ROA was under direct control. (Fig. 5 D). For the range of bar speeds that we explored the ROA varies in the interval [10, 45] Hz, a bit less that the range of retinal inputs explored in the previous section. In the common interval of variation, we observe that the AR, when it is controlled by a direct variation of the ROA (dark green curve) behaves almost linearly, similarly to the case when the retinal input is tuned by the bar speed (dark green curve), although with a smaller slope in this case. In contrast, the ML decreases non linearly, and goes to saturation when the ROA is directly tuned (red trace) whereas it decreases sharply and slightly non linearly in the case where the ROA is tuned by the bar speed (brown trace). This evidences that the decay in ML and AR versus the bar speed is not only due to the decay in the ROA but includes additional, non linear effects.

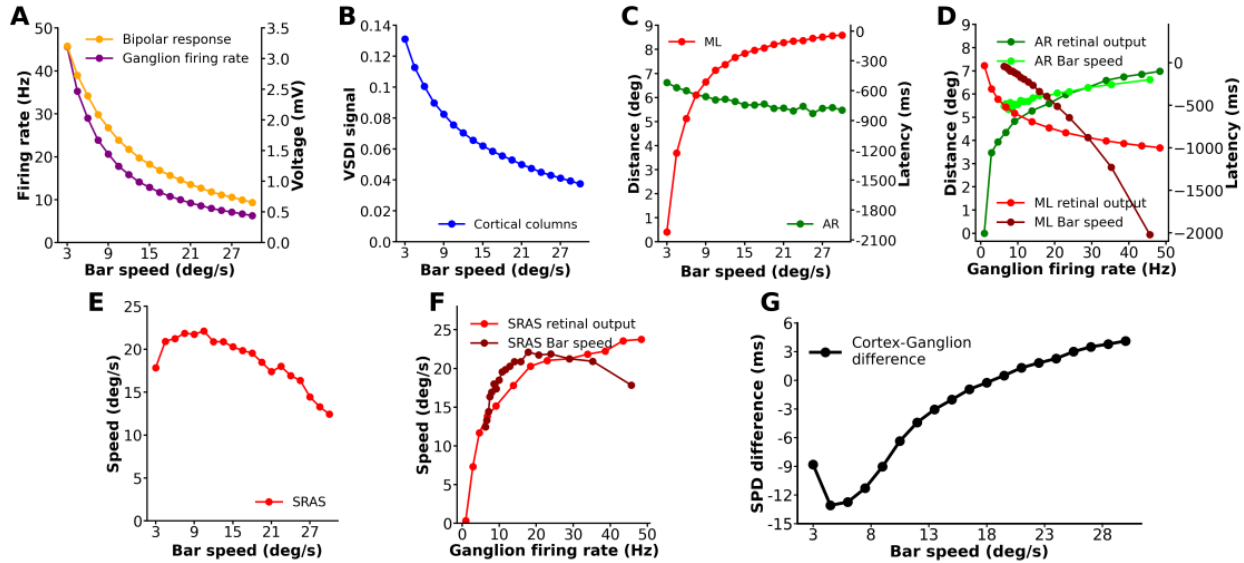


Figure 5: **The effect of the bar speed on the cortical response.** **A)** decay of the BC voltage peak and RGC firing rate (ROA) as the bar speed increases. **B)** VSDI signal amplitude of the central cortical column. **C)** **Temporal and spatial observables:** maximal latency (red) and anticipation range (green) in function of the bar speed. **D)** **ML and AR as a function of the RGC firing rate**, in the case where the firing rate is constrained by the retinal input (red for ML, dark green for AR) and in the case where the firing rate is constrained by the bar speed (brown for ML, light green for AR). **E)** **Speed observable** : short-range activation speed (red) versus the bar speed. **F)** **SRAS as a function of the ganglion firing rate**, in the case where the firing rate is constrained by the retinal input (red) and in the case where the firing rate is constrained by the bar speed (brown). **G)** **SPD difference** between cortical VSDI and ganglion firing rate.

Similarly, we studied the effect of the bar speed on the SRAS, Fig. 5 E. This quantity shows an increase up to  $9^\circ/s$  (2.7 mm/s in the retina, 27 mm/s in the cortex), then a decrease, suggesting the existence of a range of preferred speeds where anticipation by latency is optimal. Note that this effect cannot be explained only by the decrease of the ROA, as shown by Fig. 5 F. The red trace (direct control of ROA) is rather different from the curve where ROA is controlled by the bar speed (brown trace).

One actually expects three distinct effects as the bar speed increases. First, a decrease of the VSDI signal, since the OPL convolution kernel has less time to integrate the stimulus, directly impacting the anticipation. Second, a cortical column integrates the retinal signal as well but if the speed of the bar is very small (say, even static) its response occurs within a characteristic time quite shorter than the time it takes to the bar to reach the next column. In other words, when the bar arrives to the next column, the activity coming from the previous one has dropped to zero. This does not allow the columns to build up a non linear propagating front travelling faster than the bar. As the bar speed increases this front takes place and anticipation gradually increases. However, the lateral cortical connectivity has less time to build up long range excitation. Thus, as a third effect, the activity generated by this bar eventually catches up the one carried by the lateral connectivity. In consequence, the speed of anticipation is gradually overwhelmed by the speed of the bar. This last effect explains the maximum observed in the SRAS. Beyond this point anticipation by latency is more and more driven by the decay of the VSDI signal, as the bar speed approaches the conduction speed (although we are far from this limit in our bar speed range).



Finally, we investigated the role of the bar speed on the anticipation by peak shift (Figs. 5 G). The SPD shows up a minimum at about  $4.1^\circ/s$ , where the advance of the cortical SPD with respect to the RGC SPD is maximal. After this minimum there is a non linear, sigmoidal like, increase of the SPD, which switches from negative to positive at about  $16^\circ/s$ . Thus, for larger speed, the cortical peak is delayed with respect to the RGC peak. This effect of the SPD can be explained as follows. An increase in the speed causes a reduction in the RGC response (Fig. 5 A) and cortical SPDs before stabilising above  $9^\circ/s$ . The RGC SPD actually stabilizes at a time which is nearly the characteristic integration time of the RF, about 100 ms, as expected from a direct integration of (1). This explains the observed saturation.

To sum up increasing the bar speed first decreases the amplitude of the retinal input. In parallel, one observes a monotonous decrease of ML and a (moderate) decay of AR. However, this detrimental effect on anticipation is not only due to the decay of the output; additional, non linear effect take place. This is prominent when observing the SRAS which shows a "preferred" speeds range (at about  $9^\circ/s$ ) where it is maximal. This preferred speed is also the place where the SPDs of RGCs and cortex saturate. We also observe a slight anticipation by peak shift (overwhelmed by anticipation by latency) with a "preferred" speed at about  $4.1^\circ/s$ .

### 3.2.3 The role of excitatory and inhibitory connections length on cortical anticipation

We have next explored the influence of the excitatory and inhibitory connectivity lengths on cortical anticipation, an effect which cannot be studied experimentally (Fig. 6). We need to recall first a salient feature of the model. The cortical connectivity is modeled by a *normalized* Gaussian kernel (section 2.2, eq. (11)) where the cortical extent (excitatory or inhibitory) is the mean square deviation of the Gaussian. As a consequence, the shorter the cortical extensions, the more the Gaussian connectivity profile is concentrated around the cortical column's receptive field, with a higher weight. Inversely, increasing the cortical extensions spreads the Gaussian and reduces its weights. Therefore, acting on the Gaussian mean square deviation dramatically influences the value of the mean cortical column voltage for the excitatory and inhibitory populations as well as their polarisation in the steady state, with, thereby a significant impact on the VSDI signal, AR, and ML. This is illustrated in Fig. 6.

We maintained the ratio between the two respective lengths to a constant ratio of 0.2 so as to keep the balance between excitation and inhibition extents. The excitatory extent was then varied from  $1^\circ$  to  $7^\circ$  and the inhibitory extent from  $0.2^\circ$  to  $1.4^\circ$ . The first prominent effect, observed in Fig. 6 A, is the behaviour of the VSDI signal. In contrast to the previous cases, it is non monotonous. It decays up to a minimum at about  $2^\circ$  before increasing. To better understand this behaviour we have plotted, in Fig. 6 E, the peak of the excitatory mean voltage (called  $\mu_{V,E}$  in the appendix 5.2) as a function of the excitatory cortical extent (dark green) while the light green curve represents the excitatory mean voltage at rest. The difference between the two, "mean voltage difference", is shown in Fig. 6 F (dark green). Likewise, Fig. 6 G shows the peak of the inhibitory mean voltage (brown) and inhibitory mean voltage at rest (red), while the red trace in Fig. 6 G shows the difference between these two quantities. The total VSDI signal as a function of the cortical extent is a linear combination of these two traces, (eq. (22), appendix 5.2).

When the cortical extent increases from  $1^\circ$  up to  $2^\circ$  we observe that the excitatory and inhibitory mean voltages increase while the mean voltage differences decreases, explaining the observed decay of the VSDI signal. This decrease is due to the fact that the mean voltage at rest increases faster than the peak mean voltage, for both population. As anticipated above, this behaviour can be explained by the Gaussian connectivity profiles. Increasing the cortical length decreases the intensity of the coupling between two cortical columns. Short extensions give a concentrated Gaussian with strong weights but short range influence. When the inhibitory cortical extent is  $0.2^\circ$  (resp.  $1^\circ$  for the excitatory cortical extent), the inhibitory Gaussian is so concentrated that its weight far exceeds that of the excitatory. This inhibitory dominance gives rise to a strong steady-state hyperpolarisation and an overall sensitisation of the cortical column which reacts more strongly to the stimulus. This hyperpolarisation is reduced by the elongation of the inhibitory extensions above  $0.2^\circ$ . This mean vorage difference decreases leading to a reduction in the VSDI. From  $2^\circ$ , we observe a decay in the steady state voltage for excitatory and inhibitory population, corresponding to a new phase of hyperpolarisation at rest. When the cortical extent increases, the excitatory and inhibitory weights decrease thereby diminishing the mean voltage at rest. In contrast, the mean voltage peak increases for excitators and have a moderate variation for inhibitors. As a consequence, the mean voltage differences increase, leading to an increase of the VSDI.

We observe a positive effect on anticipation by latency since AR and ML increase when the cortical extent increases (Fig. 6 B) as well as SRAS (Fig. 6 C) with a saturation for an excitatory and inhibitory length respectively at  $7^\circ$  and  $1.4^\circ$ . Here, it is interesting to note that the measured AR is always larger than the length of the corresponding excitatory connectivity (black dotted line, Fig. 6B). The cortical columns are therefore influenced beyond the excitatory extent, and, therefore also earlier, promoting anticipation. This is particularly true up to  $4^\circ$  where this effect is maximal. Beyond  $7^\circ$ , the AR and ML start to saturate. We believe that this arises because the Gaussian extent increases at the expense of proximity activity until the weights on the periphery of the Gaussian become insufficient to activate the cortical columns, corresponding to this limit of  $7^\circ$ .



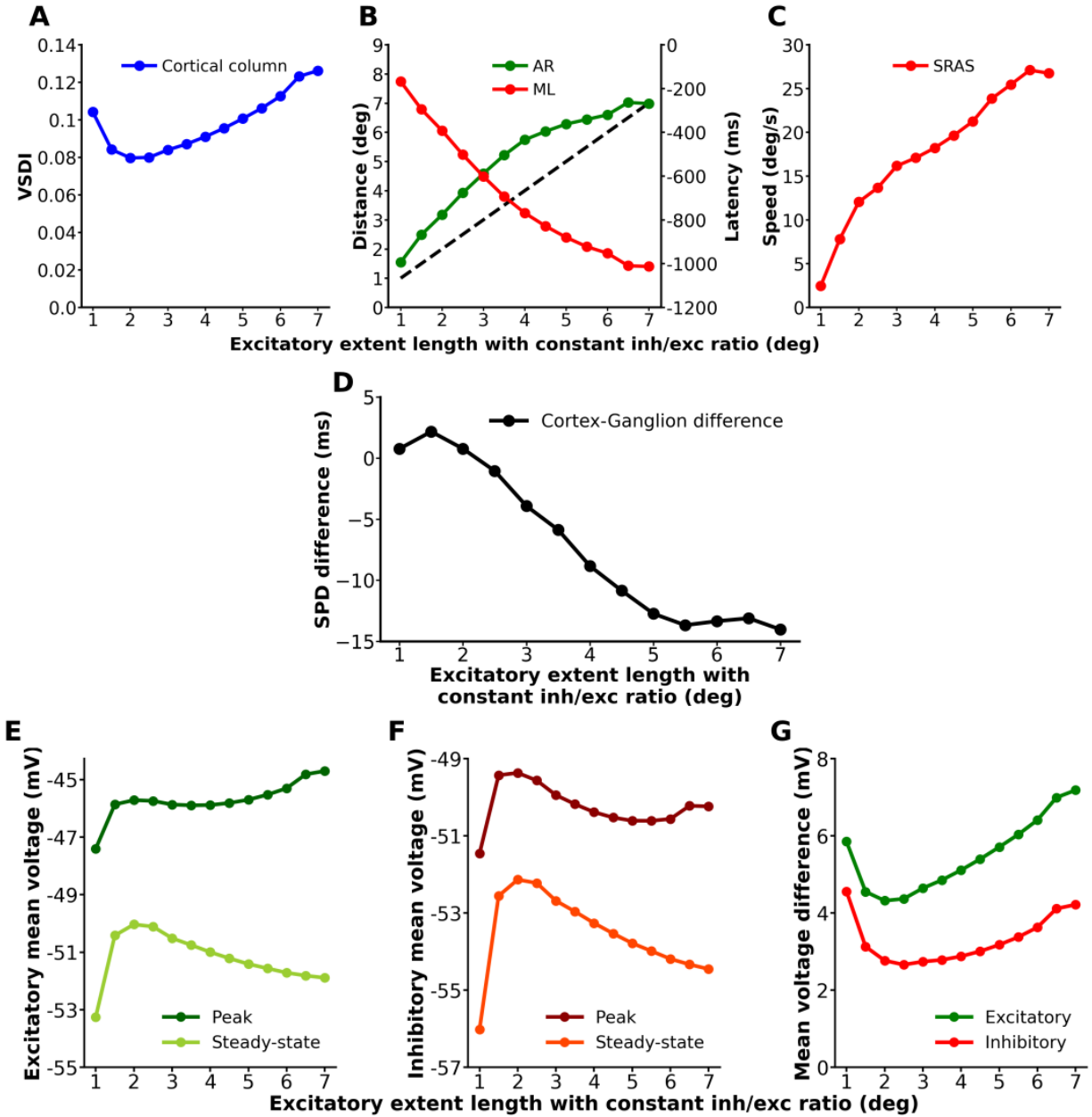


Figure 6: **The effect of excitatory and inhibitory connectivity length on the cortical response.** In the whole figure, the variable on abscissa is the excitatory cortical extent, but recall that there is a constant ratio with the inhibitory extent. **A) VSDI signal amplitude** of the central cortical column versus the cortical extent length. **B) Temporal and spatial observables:** anticipation range (green) and maximal latency (red) in function of excitatory. The black dotted line represents the equality between distance and length of excitatory connectivity. **C) Speed observable :** short-range activation speed (red) in function of excitatory extent. **D) Difference** between RGC SPD and VSDI signal SPD. **E) Excitatory mean voltage** at the peak (dark green) and at the steady-state (light green). **F) Inhibitory mean voltage** at the peak (dark red) and at the steady-state (light red). **G) Mean voltage peak amplitude** for excitators (green) or inhibitors (red). This is the difference between the average peak voltage and the steady state voltage.

We observe that the SPD is also affected by the increase in cortical extent, Fig. 6 D. For cortical extent smaller than  $2^\circ$  the cortical peak is delayed with respect to the RGC peak. In particular, as the connections length tends to 0, the SPD difference (black trace) in Fig. 6 tends to 0. This justifies our comment in section 3.2.1 where we claimed that the difference between RGC and VSDI SPD is primary due to the cortical lateral connectivity. Beyond  $2^\circ$  the cortical SPD

decreases (while the RGC SPD obviously stays constant), Fig. 6 D, so that the VSDI signal peak is more and more in advance to the RGC peak with a saturation at about  $5^\circ$ . The time scale of this peak delay (maximum  $-14$  ms) is quite lower than the ML though.

Therefore, anticipation is enhanced by increasing the length of excitatory and inhibitory fibres at a constant ratio for values inferior to  $7^\circ$ . This improvement also involved an earlier shift in the VSDI peak. These effects are highly dependent on changes in the Gaussian profile. The effect is the strongest with an excitatory length of  $4^\circ$  and an inhibitory length of  $0.8^\circ$ . This is close to the physiological connectivity that we use in the rest of the paper.

### 3.2.4 The role of conduction velocity

We finally investigate the influence of fibre conduction velocity between cortical columns on anticipation in control conditions (Figure 7), in the range  $100 - 333^\circ/s$ . The effects are rather easy to resume and are shown in Fig. 7. There is no effect on the VSDI signal. The ML slightly decreases while the AR slightly increases. More interesting is the behaviour of SRAS which is increasing almost linearly. In the paper [8] Benvenuti et al. proposed a phenomenological, physiologically plausible model of lateral cortical integration in response to a moving bar (Fig. 3 of their paper). In their model, SRAS increases linearly with a 1:1 ratio to the fibre conduction speed (Fig. 3D of their paper). In our model, which integrates more biological features, we also observe a (quasi)-linear behaviour but the slope,  $\sim 0.035$  is far from 1. In our opinion, this is because they only used lateral excitation while inhibitory lateral connectivity also plays an important role. Inhibition acts as an impediment to the activation of cortical columns, explaining the small slope. The increase in fibre conduction speed is also accompanied by a very slight decrease of 0.6 ms in the shift between the cortex and the ganglion cells SPD (7 E).

To sum up, the only remarkable effect induced by an increase in the conduction velocity is a linear increase in the SRAS, similar to what has been conjectured by Benvenuti et al in [8], but with a quite smaller slope, due to lateral inhibition.

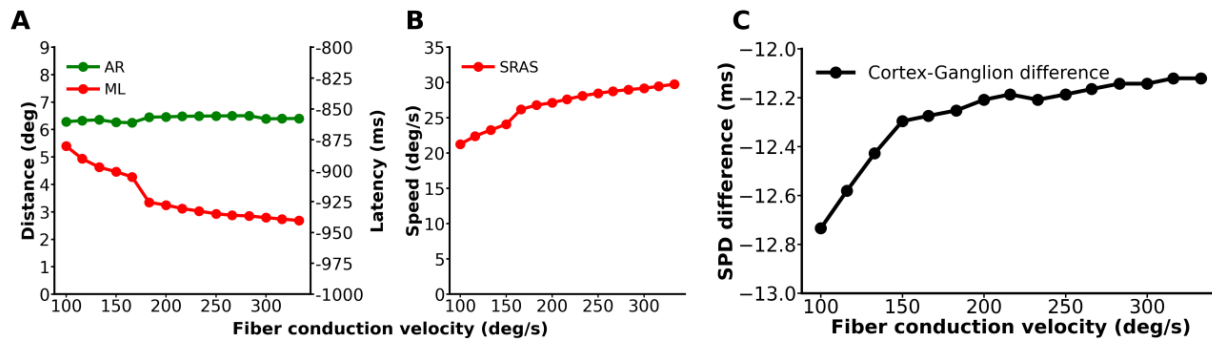


Figure 7: **The effect of fibre conduction velocity on the cortical response** **A) Temporal and spatial observables:** anticipation range (green) and maximal latency (red) in function of excitatory and inhibitory extent. **B) Speed observable:** short-range activation speed (red) in function of fibre conduction velocity. **C) Difference** between RGC SPD and VSDI signal SPD.

### 3.2.5 Conclusion of section 3.2

We have shown that our cortical model can reproduce the cortical anticipation observed experimentally, although with some quantitative discrepancies, and explored effects that cannot be studied in an experimental setting. The anticipation in our model clearly results from the propagation of activity in an excitatory/inhibitory balanced horizontal network. We have also shown that, in addition to latency, cortical anticipation has a peak shift component. The ability of this system to anticipate is closely linked to a few parameters. Increasing the amplitude (Fig. 3) or the length of connectivity at a constant inh/exc ratio (Fig. 6) improves the ability to anticipate by shift and latency. On the contrary, increasing the speed of the bar (Fig.5) first increases anticipation then decreases it, beyond a "preferred speed". Finally, increasing the conduction velocity of cortical fibres (Fig.7) allows anticipation to propagate more rapidly in the cortex, as expected. This propagation remains limited by inhibition though.

## 3.3 Cortical anticipation is influenced by the retina

We now investigate how the cortical response behaves if the retinal drive is itself generating peak anticipation during the integration of the motion. Our retina model first implements gain control following [1, 14]. This has the effect of

advancing the peak response of ganglion cells' activity. The effect increases with the size and the contrast of the bar while it decreases with its velocity [20, 21]. Anticipation in the retina can also be studied from the point of view of the population, taking into account the interactions between the different cells. We have therefore implemented amacrine cell connectivity and designed a retinal circuit capable, under certain conditions, of improving retinal anticipation. Theoretical and numerical results concerning the role of lateral connectivity in retinal anticipation of motion trajectories can be found in [20, 21]. Note that, in general, these mechanisms generating peak anticipation also modify the time profile of the RGCs response to the moving bar (see Fig. 8 E, 10 E). The resulting effect on the cortical response is thus not only a shift in the VSDI signal peak, but a change in its global shape as well (see e.g. Fig. 8 F, 10 F or Fig. 12). This entails potential changes in the VSDI signal amplitude and in the latency. In general, the global effect is quite entangled.

Gain control and amacrine cells connectivity cause, on one hand, a decrease in the ROA, and on the other hand, a shift of the response peak earlier while changing its shape. Now, as we saw above, decreasing the amplitude of the retinal input impacts the cortical response. Thus, to isolate the effect of e.g. gain control on anticipation we need to compare the situation with gain control to the situation with no gain control, while the ROA are identical. The set of control simulations where no effect (gain control or amacrine cells network) is present, but where the amplitude of the retinal input is rescaled to match the case where the effect is present is called "equivalent retinal output amplitude" (EROA).

### 3.3.1 Gain control in the retina enhances cortical anticipation

In the model, gain control can be present in BCs or RGCs. We ran simulations with increasing values of the strength of these two gain controls and compare these results to EROA conditions.

**Variation of BCs gain control.** We first simulated the response to the moving bar with a bipolar gain control (parameters  $h_B$  in eq. (2)) varying between 0 and 9.2 mV/s. As shown in [20, 22] gain control triggers the appearance of adapting anticipation in the cortex. We investigate here what is the induced effect on cortical anticipation, by latency and by peak shift.

The increase in  $h_B$  is first associated to a moderate decrease in the amplitude of the VSDI signal (Fig 8A). This was expected since the strength of gain control in BCs reduces the amplitude of the retinal response. We observe however a slight deviation of the VSDI signal compared to the EROA condition: the amplitude of the VSDI signal remains larger. This is because, when  $h_B$  increases, gain control changes the shape of the BC response (not shown) and thereby the RGC profile integrated by the cortex (Fig. 8 E, F). Anticipation by latency (AR and ML) is slightly favoured for small values of  $h_B$  ( $\leq 4.3$  mV/s) before being attenuated. There is no difference with EROA for AR. In the case of the ML, the decreasing regime is less marked than for EROA condition. For a gain control of 9.2 mV/s, ML increases by 7.6% more than EROA (Fig. 8 B). This indicates an additional positive effect of gain control on ML, which partially compensates for the anticipation decay due to retinal amplitude output reduction. The SRAS increases much more than in the EROA condition (Fig. 8 C). In comparison, it is 26.7% faster than the speed observed in EROA for BCs gain control at 9.2 mV/s. This effect is strong enough to compensate and even reverse the slight decrease due to the reduction in the amplitude of the retinal input.

Concerning the anticipation by peak shift, the presence of BCs gain control results in a  $-77$  ms ( $-51.5\%$ ) increase in RGC SPD between  $h_B = 0$  and  $h_B = 9.2$  mV/s (Fig. 8 E). This is accompanied by an earlier shift in the cortex peak of  $-72.5$  ms ( $-53\%$ ) (Fig. 8 F), corresponding to a strong anticipation by peak shift. Note the difference in the response profiles for  $h_B = 0$  (red traces) and  $h_B = 9.2$  mV/s (green dashed traces) in the RGC response and in the VSDI response. Fig. 8 D illustrates the evolution of the RGC SPD (orange trace), the cortical SPD (blue trace), and the difference of these two quantities (black trace). This difference shows a maximum at  $h_B = 4.9$  mV/s.

To sum up, this study demonstrates the direct influence of retinal peak anticipation on the cortex when increasing the BCs gain control. BCs gain control induces a earlier shift of the RGC peak, a reduced amplitude in the retinal input, and a change in the RGC response profile, with a corollary anticipation in the VSDI signal, by adaptation and by latency. However, the impact on anticipation depends on the level of BCs gain control. For small  $h_B$  ( $\leq 4.9$ ) the main effect is an increase in the peak shift with no significant effect on the cortical anticipation by latency. For larger  $h_B$  anticipatory waves propagate faster (SRAS) than in EROA condition but with a reduced latency (ML) and a reduced range at which cortical columns begin to anticipate (AR). Large  $h_B$  lead to a reduction in the peak shift of the cortex, detrimental effects on ML and AR, while SRAS saturates. This suggests therefore that there is an optimal value for BCs gain control.

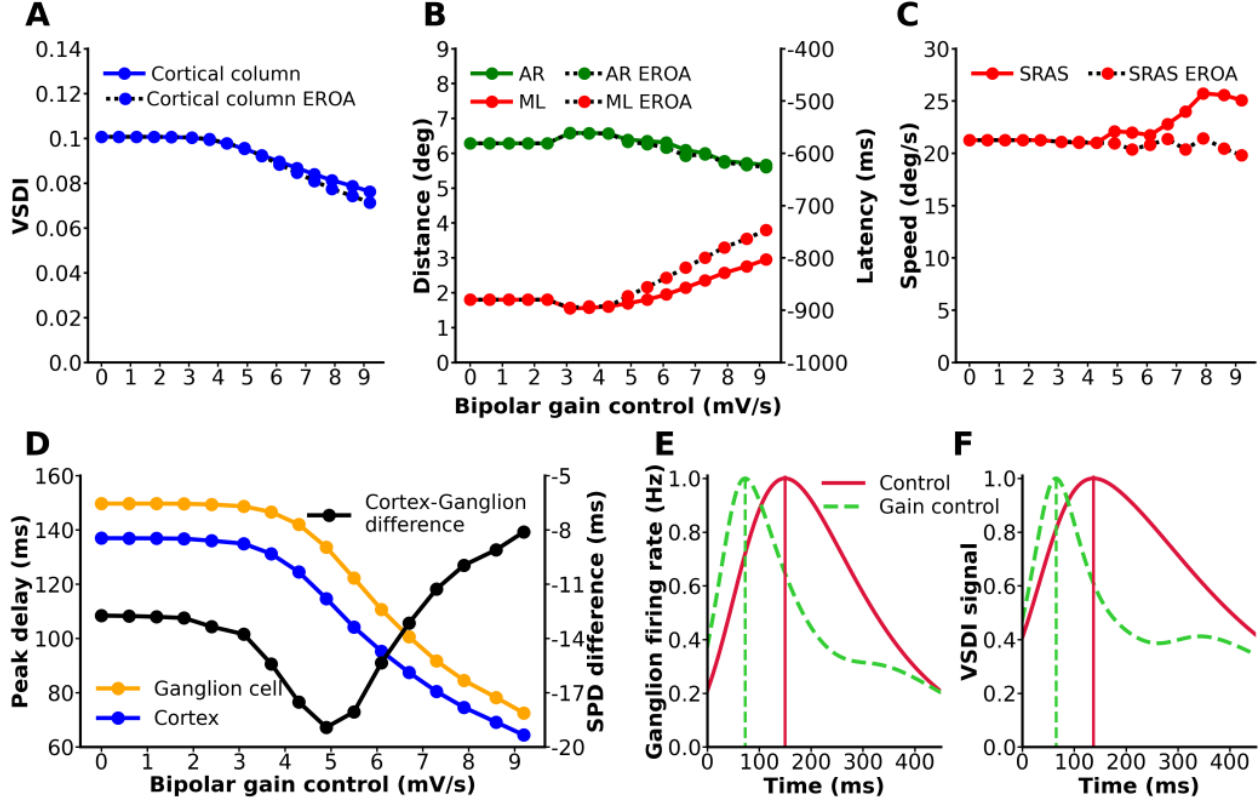


Figure 8: **The effect of bipolar gain control strength,  $h_B$ , on the cortical response.** **A)** VSDI signal amplitude of the central cortical column versus  $h_B$ . **B)** Temporal and spatial observables: anticipation range (green) and maximal latency (red) versus  $h_B$ . **C)** Speed observable : short-range activation speed (red) in function of bipolar gain control weight. In A, B, C, we also draw the Equivalent Retinal Output Amplitude (EROA) curve. This is the dotted black curve with the same coloured symbols. **D)** SPD for RGCs (orange), VSDI signal (blue) for the central cell (scales on the left) and difference between RGC SPD and VSDI signal SPD (black, scales on the right). **E)** Shape of the central RGC response profile to the moving bar, without gain control (red) and with BC gain control (dashed green). Note that the two traces have been rescaled to have the same maximum. This is to emphasize the change in the shape of the response induced by BCs gain control. **F)** VSDI signal, same conditions. In E,F, the dotted lines correspond to the peaks in the RGC firing rate or VSDI signal without BCs gain control (red) and with it (green).

**Variation of RGCs gain control.** Here, we varied the RGCs gain control,  $h_G$ , from  $0.18 \text{ mV}^{-1}\text{Hz}$  to  $0.54 \text{ mV}^{-1}\text{Hz}$  (Fig. 9). Note that the range of values is very different from BCs gain control because the non linearity in the gain function is quite different (see eq. (5) versus (8)). The result shows strong similarities with BCs gain control though. The first similarity is that the stronger the gain control, the lower the VSDI signal (Fig. 9A) with a similar range of values, although the decay of the VSDI signal curve is identical to the EROA condition and has a different profile than for BCs gain control. As a second similarity, the RGCs gain control reduces AR and ML (Fig. 9B). However, this reduction is steeper and monotonous. Compared to EROA condition, AR remains unchanged while ML increases slightly (6.1% at  $0.54 \text{ mV/s}$ ). The SRAS curve shows, in contrast, a big difference with the bipolar case. SRAS increases up to  $h_G = 0.29 \text{ mV/s}$  before decreasing slightly (Fig. 9C). The EROA curve shows a smaller increase and a larger decrease. RGCs gain control has therefore a positive effect on SRAS (21.9% at  $0.54 \text{ Hz}$ ). This effect is opposed to the negative effect of retinal amplitude reduction. Below  $0.29 \text{ mV/s}$ , the positive effect predominates before being overwhelmed by the reduction in retinal amplitude.

We observe an increase in the peak shifts in the retina and in the cortex by the addition of RGCs gain control. The RGCs arises  $50.5 \text{ ms}$  earlier for  $h_G = 0.54 \text{ mV/Hz}$  compared to control conditions,  $h_G = 0$  (Fig. 9E) while the cortical SPD occurs up to  $52 \text{ ms}$  earlier ( $-38.1\%$ ) in the cortex (Fig. 9F). As shown by Fig. 9D, when  $h_G$  increases, the RGC SPD (orange trace) decreases as well as the cortical SPD (blue trace), while the difference between the two decreases for small values of  $h_G$  ( $< 0.1 \text{ Hz/mV}$ ) and then stays constant (black trace). Fig. 9E, F also reveals a major difference with BCs gain control (compare to Fig. 8 E, F): the response profile of RGCs and cortical columns is quite less modified

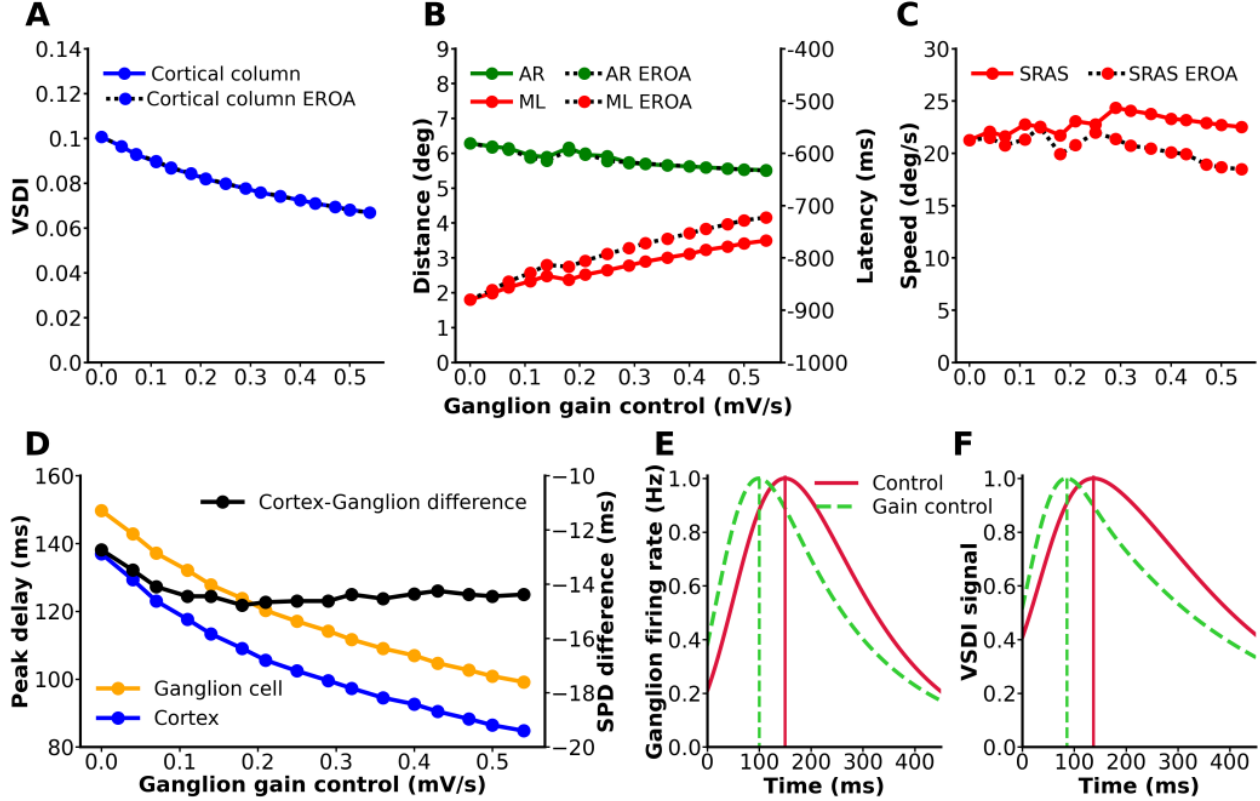


Figure 9: **The effect of RGCs gain control strength,  $h_G$ , on the cortical response.** The representation is the same as in Fig. 8

than in the case of BC gain control. Essentially, RGC gain control only entails a peak shift. In contrast BCs gain control induces a cascade of convolutions up to the RGC, modifying the RGC response profile and the VSDI signal.

To conclude, the RGCs gain has a negative effect on cortical anticipation by latency while transferring the adaption anticipation coming from the retina and enhancing the intrinsic cortical shift. SRAS shows also some improvement in the presence of RGC gain control. A similar compensatory effect is observed in ML (compared to EROA), but not sufficient to compensate the decrease in ML. Finally, we mentioned in section 3.1 that the time of the peak in CTL conditions is located at 139 ms, while the peak observed in experiments (Fig. 4D of [8]) is very close to 0. We proposed that the discrepancy ought to be due to the absence of retinal anticipation mechanisms in CTL conditions. Here we see that combining the maximal peak shift due to BCs gain control ( $-72$  ms) and the peak shift due to RGCs gain control ( $-52$  ms) we arrive at a cumulative peak shift of  $-134$  ms, so that, compared to CTL, the time to peak with gain control is close to 0, as observed in experiments.

### 3.3.2 The anticipatory role of amacrine cells

Here, we study the effect of lateral ACs inhibition. ACs, like horizontal cells, provide a lateral connectivity somewhat entangling the "vertical" information channels from photoreceptors to retinal ganglion cells via bipolar cells. Although some ACs can have excitatory connections (e.g. cholinergic) we mainly focus here on inhibitory effects of ACs. Amacrine cells constitute networks which modulate and can potentially propagate the response of BCs to a moving signal to other BCs and RGCs. This depends though crucially on the scaling between synaptic weights ( $w_B^A, w_A^B, w_G^A, w_G^B$  in the model) and characteristic integration times ( $\tau_A, \tau_B, \tau_G$  in the model). A detailed study in [10] shows that tuning these parameters dramatically change the shape of the response to simple flashes (e.g. from monophasic response to biphasic), while [20, 22] emphasize the effect of stimulus induced wave propagation leading to an advancement of the peak time in RGCs. The network response to the moving bar also depends on the connectivity structure. By construction, our model has a feedback connectivity where BCs act on ACs which modulate BCs back. But, one can also study a feed-forward case where BCs input ACs without reciprocal connection, simply by setting  $w_B^A = 0$ . S. Ebert [13] shown in her thesis that the response is rather different. Especially, with feedback connections ACs can

induce effects similar to BCs gain control while modifying the spatio-temporal BC response (e.g. leading to biphasic or polyphasic responses even if the OPL input is monophasic [10]). The aforementioned studies were focusing on anticipation at the retinal level. Here, we analyse the impact on cortical anticipation, along the same lines as the previous sections, feed-forward versus feedback inhibition.

**Feed-Forward amacrine inhibition.** We study first the direct influence of feed-forward inhibition pathway with connectivity from BCs to ACs and from ACs to RGCs, respectively characterized by the parameters  $w_A^B$  and  $w_G^A$  in eq. (2). We varied  $w_G^A \leq 0$ , controlling the intensity of ACs synapses to RGCs, and  $w_A^B \geq 0$ , controlling the intensity of BCs synapses to ACs, from 0 to 1 Hz, restricting to the case  $w_G^A = -w_A^B$ . The other parameters are tuned to the control value (appendix 5.1). The results are shown in Fig. 10. As expected, the inhibitory effect of ACs induces a decrease in the VSDI signal amplitude (Fig. 10 A). Note that the VSDI signal curve in this condition is essentially indistinguishable from the EROA curve, confirming that the effect of ACs on VSDI, in feedforward conditions, is only a drop in the amplitude of the retinal input. Fig. 10 B shows a detrimental effect of forward inhibition on the AR, as well as on the ML, although less important than in EROA. In contrast, the comparison of the SRAS obtained with feedforward inhibition and its corresponding EROA reveals a compensatory effect of the retinal amplitude. While EROA decreases fast, SRAS remains relatively constant suggesting a mechanism which counterbalances the decrease in speed due to the decrease in amplitude.

The most prominent effect occurs on the SPD of RGCs (orange trace) and VSDI signal (blue trace) which decrease sharply (Fig. 10 D), though with a difference becoming smaller and smaller in absolute value (black trace). These behaviors are accompanied by a strongly advancement of  $-104$  ms ( $-69.4\%$ ) for the RGC spd (Fig. 10 E) and of  $-88$  ms ( $-64.2\%$ ) for the VSDI signal peak (Fig. 10 F), when  $|w_G^A| = w_A^B = 1$  Hz. Note that we observe also a small rebound of the VSDI signal (Fig. 10 F), arising when  $|w_G^A|$  becomes large. When the bar arrives in their receptive field, BCs activity increases, increasing the ACs activity and their inhibitory effect on the RGC. When  $|w_G^A|$  is large enough it takes over the excitation from BCs and the RGC firing rate drops to 0. Because the ACs have here a shorter time scale than BCs (corresponding e.g. to the peak of the green dashed curve in Fig. 10 E), their effect lasts shorter and the rebound corresponds to the residual activity coming from BCs.

Thus, the presence of feedforward inhibitory connectivity implements adapting anticipation within the cortex, with an increasing effect as the intensity the synaptic weights increases, while severely penalising cortical latency anticipation (AR, ML) and intrinsic cortical shift. Surprisingly, though, the speed of the anticipatory wave remains stable thanks to compensation for the decay of the amplitude of the retinal input. All these effects are not simply due to a decrease in the ROA but entail additional effects presumably due, as for gain control, to the difference in the BCs response profile.

**Amacrine feedback inhibition.** The feedback loops BCs  $\rightarrow$  ACs  $\rightarrow$  BCs induce a complex interaction between the moving object, the local cells response and the influence of these cells on distant cells, propagated via the lateral amacrine inhibition. The picture is that of a moving bar propagating in a non homogeneous landscape of activities modulated by the amacrine network. This entails specific effects, not present with a feedforward connectivity, such as the existence of resonant frequencies [9], a change in the shape of BCs response [10] or the existence of a preferred speed range at which anticipation by adaptation is maximal [13]. In addition, the feedback loop propagates inhibition producing a decay of the response before and after the peak. This actually differs from gain control, which only acts on the post-peak portion of the curve. It has been shown that these feedback effects can be characterized by (1) the characteristic integration times of BCs ( $\tau_B$ ) and ACs ( $\tau_A$ ); (2) the average intensity of the connection from BCs to ACs,  $w_A^B \geq 0$ , and ACs to BCs,  $w_B^A \leq 0$ . Actually, the relevant parameter is  $\mu = -w_B^A w_A^B \tau^2$ , where  $\frac{1}{\tau} = \left| \frac{1}{\tau_B} - \frac{1}{\tau_A} \right|$ . In particular, this shows that the synaptic weight effects of the feedback loop is characterized by the product  $w_B^A w_A^B$ . Here, we keep  $\tau_A, \tau_B$  constant and vary  $w_B^A$  with  $w_A^B = -w_B^A$  from 0 to 12 Hz. The values of the other parameters are given in the Appendix 5.1. The goal here is to show an example of the potential effects of this type of connectivity while a more exhaustive study would require to vary other parameters as well, a task well beyond the scope of this paper.

The result of our simulations are shown in Fig. 11. The amacrine feedback loop primarily drops the amplitude of the VSDI signal with no significant difference from the EROA (Fig. 11A). It also influences the ML as well as AR (Fig. 11B) with a slight optimum. A comparison with the corresponding EROA curve reveals a negative effect of the feedback loop in addition to that caused by the reduction in the amplitude of the retinal input, particularly for AR ( $-9.1\%$  at 12 Hz) but also for ML ( $-3.7\%$  at 12 Hz). On the opposite, the SRAS is a little bit higher. This increase contrasts with the reduction observed in the EROA condition. At 12 Hz, the difference with EROA is  $39.3\%$ . This indicates a compensation of the retinal input decay by the amacrine feedback loop. This compensation counterbalances up to 6 Hz before being overtaken. The simulations also reveal an earlier SPD shift of  $50$  ms ( $-36.6\%$ ) for RGCs (Fig. 11E) transmitted to the VSDI signal. We actually observe in Fig. 11E and F, as in the previous section, a change in the shape of the RGCs response and VSDI (green traces), compared to control (red traces). The SPD for RGCs and VSDI signal,



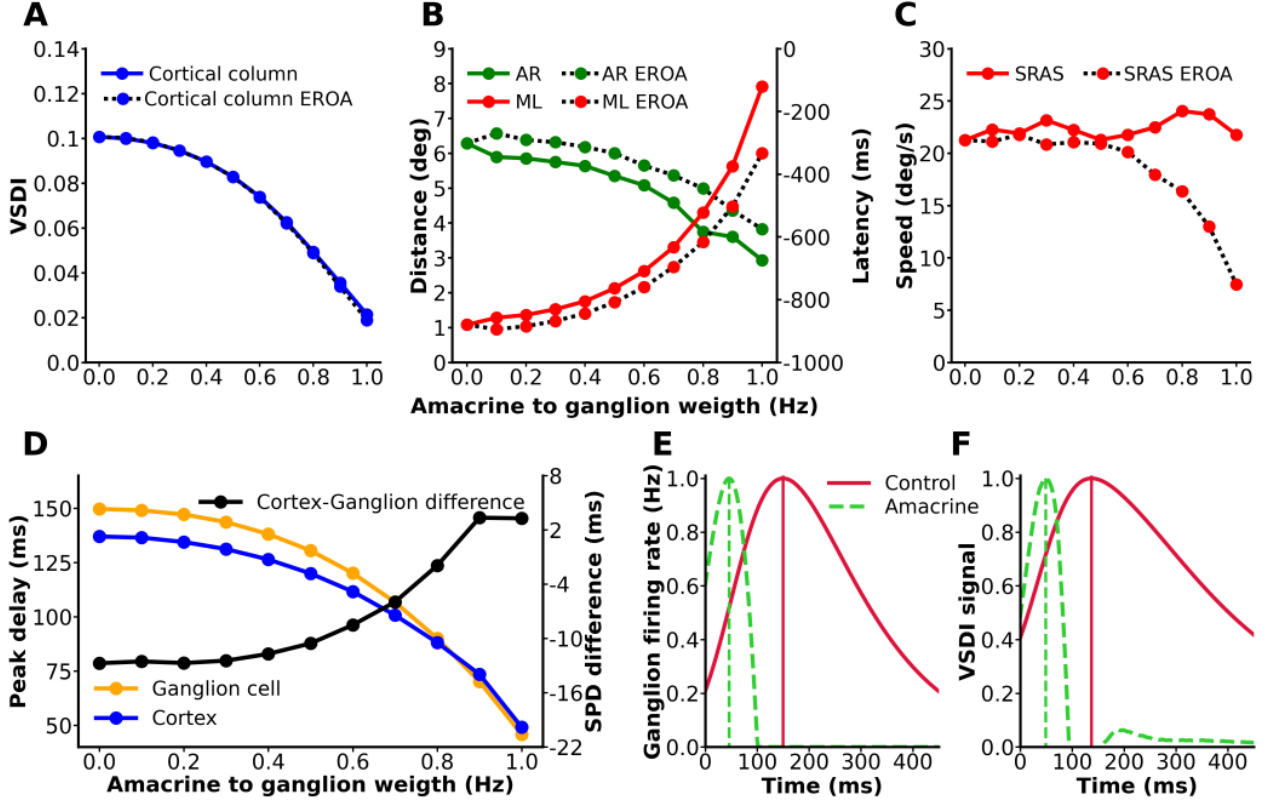


Figure 10: **The effect of forward inhibition, controlled by  $w_G^A = -w_A^B$ , on the cortical response.** **A)** VSDI signal amplitude of the central cortical column. **B)** Temporal and spatial observables: anticipation range (green) and maximal latency (red). **C)** Speed observable : short-range activation speed (red). **D)** SPD for RGCs (orange), cortical columns (blue) and difference between the cortical and RGC SPD (black). **E)** Shape of the central RGC response profile to the moving bar, without feedforward AC connection ( $w_G^A = -w_A^B = 0$ ) (red) and when these parameters take the maximum value ( $|w_G^A| = w_A^B = 1$  Hz, dashed green). Note that the two traces have been normalized to have the same maximum at 1 Hz. **F)** VSDI signal, same conditions. The dotted lines in E, F correspond to the peaks in the RGC firing rate or VSDI signal without feedforward AC connection (red) and with it (green).

as well as their difference, versus  $w_B^A$  is shown in Fig. 11D. The RGC (orange trace) and cortical (blue trace) SPDs increase but their difference diminishes (black trace). This shows an increase in retinal SPD at the expense of cortical SPD. The difference is minimal at  $w_A^B = 12$  Hz but the SPD is maximal at this same connectivity value. A behavior similar to the feedforward effect but with a smoother slope.

These results demonstrate the capacity of amacrine retro-control to provoke adapting anticipation influencing the cortex. However, this is accompanied by a negative effect on cortical anticipation by latency mainly manifested by a drop in the AR, ML and of the cortical peak shift.

### 3.3.3 The anticipatory impact of the retina

We now synthesize our observations about the cortical correlates of the retinal anticipatory mechanisms. Although our investigations are absolutely non exhaustive - a more detailed study would require to vary a larger set of parameters in the model - it reveals several effects which are generic, i.e. present on a wide range of parameters value, although the *quantitative* observations may depend on these parameters. These generic effects are an advancement of the RGC output peak, a decrease in the ROA, and a global change in the shape of the firing rate response. This has an impact on the VSDI response, illustrated in the figures above and summarized in Fig. 12.

In Fig. 12 A, we compare the respective effect of BC and RGC gain control on the VSDI signal at the central cell. It is however rather difficult to compare quantitatively the effects of these two gain control mechanisms, as a systematic study would require to modify jointly  $h_B$  and  $h_G$  in a two dimensional map, a task beyond the scope of this paper. Here,

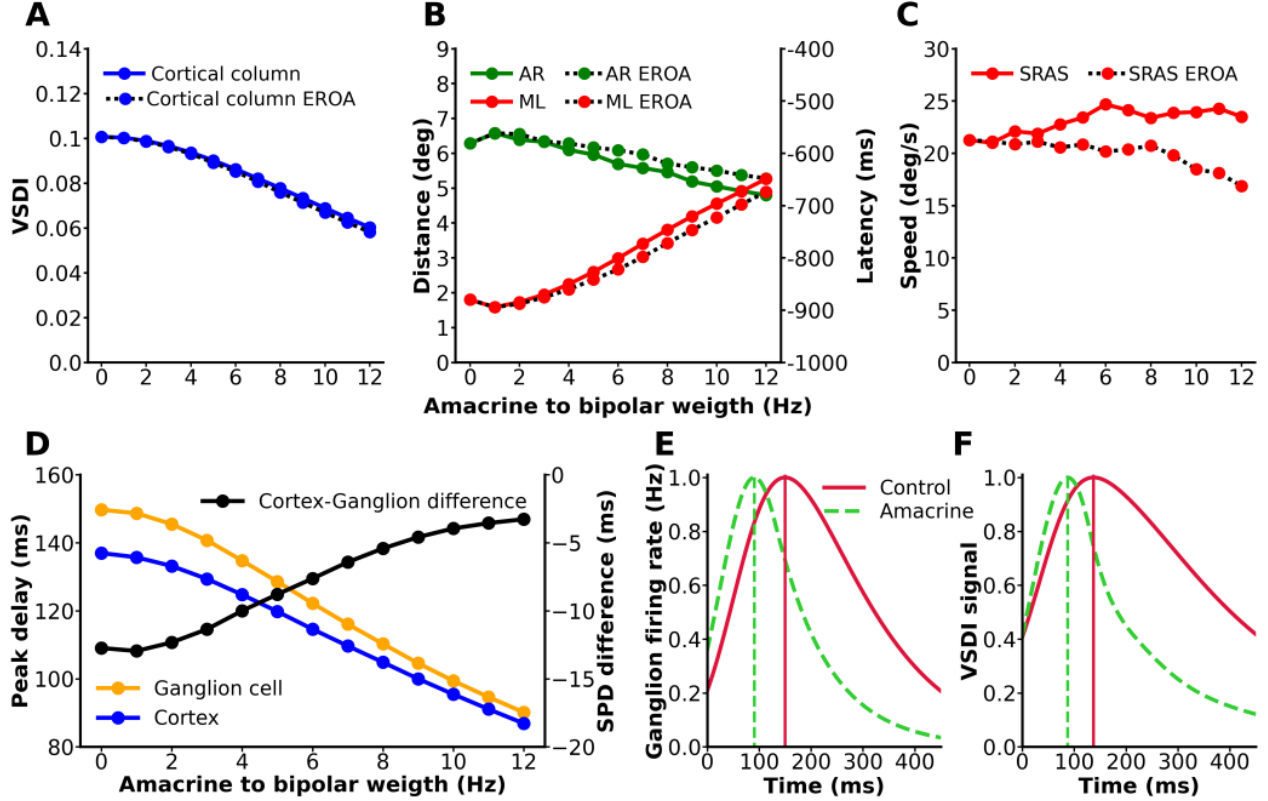


Figure 11: **The effect of ACs-BCs feedback loop on the cortical response.** **A) Amplitude quantity:** VSDI signal amplitude of the central cortical column versus the feedback loop weight. **B) Temporal and spatial observables:** anticipation range (green) and maximal latency (red). **C) Speed observable :** short-range activation speed (red) in function of amacrine to bipolar weight. **D) SPD for RGCs** (orange), cortical columns (blue) and difference between the cortical and RGC SPD (black). **E) Shape of the central RGC response profile to the moving bar,** without feedback AC connection ( $w_B^A = -w_A^B = 0$ ) (red) and when these parameters take the maximum value ( $|w_B^A| = w_A^B = 1$  Hz, dashed green). Note that the two traces have been rescaled to have the same maximum. **F) VSDI signal,** same conditions. The dotted lines in E,F correspond to the peaks in the RGC firing rate or VSDI signal without feedforward AC connection (red) and with it (green).

we only compare the model response in a case where BCs and RGCs gain control are tuned so that the retinal output amplitude is the same (ROA = 17.1 Hz), that is  $h_B = 8.554$  mV/s (magenta trace) and  $h_G = 0.359$  mV/s (yellow trace). The first observation is a peak shift stronger for BC gain control than for RGC gain control. There is a SPD difference of 25 ms (36.7%). There is also a strong difference in the VSDI signal profile, after the pic. It is unfortunately not possible to compare this with the experimental results in [8] as the VSDI profiles they show (e.g. Fig. 4 D) is cut before the place where such a possible rebound may occur. Performing new experiments on a larger time scale would be a way to confirm the role of BC gain control on the VSDI signal profile. Finally, one sees a small variation in the early part of the curves, where latency is computed. The smallness of this variation is due to the scaling of the figure though, where we wanted to show the whole VSDI profile. Now, remember that cortical latency observables are computed at the very beginning of the activity rising, when this activity exceeds a threshold of 0.001 (section 2.4). Thus, there is a small but significant effect on latency observables. There is a difference of  $-1.2\%$  for AR,  $-2\%$  for ML and  $-7\%$  for SRAS, in favour of BC gain control. This suggests that, overall, BC gain control is more effective. However, cortical anticipation by latency is slightly affected compared to adapting anticipation which is much higher. To sum up BCs control appears more effective at generating peak anticipation while limiting the impact on cortical latency anticipation and increasing the speed of anticipation.

In the same vein, Fig. 12 B compares the role of feedforward versus feedback amacrine cells connectivity, adjusting the control parameters  $w_G^A = 0.7$  Hz (feedforward) and  $w_B^A = 11$  Hz (feedback) so that the ROA are equal to 13.1 Hz. We observe here a small pic shift and a small change in latency while the main visible effect is a change in the shape of the VSDI profile after the peak. For these value of parameters, the AR actually decreases by  $-6.9\%$  when comparing the



feedback case to the feedforward case, the ML decreases of  $-6\%$  and SRAS by  $-7.3\%$ . Finally, SPD arrives 9 ms later in the feedforward case than in the feedback case (10.6%). Although the difference is rather tiny, a general conclusion would require a more systematic study. In particular, a comparison of Fig. 10 and Fig. 11 suggests a better efficiency of amacrine connectivity in the form of a feedback loop. Adapting anticipation is more pronounced while limiting the impact on cortical latency anticipation despite the smaller intrinsic cortical delay. On the basis of preliminary results obtained in [13] we actually believe that the main difference between the two effects would hold when varying the bar speed. We expect the presence of a preferred bar speed - where anticipation is maximum - in the feedback case and not in the feedforward case (where anticipation would grow monotonously until saturation).

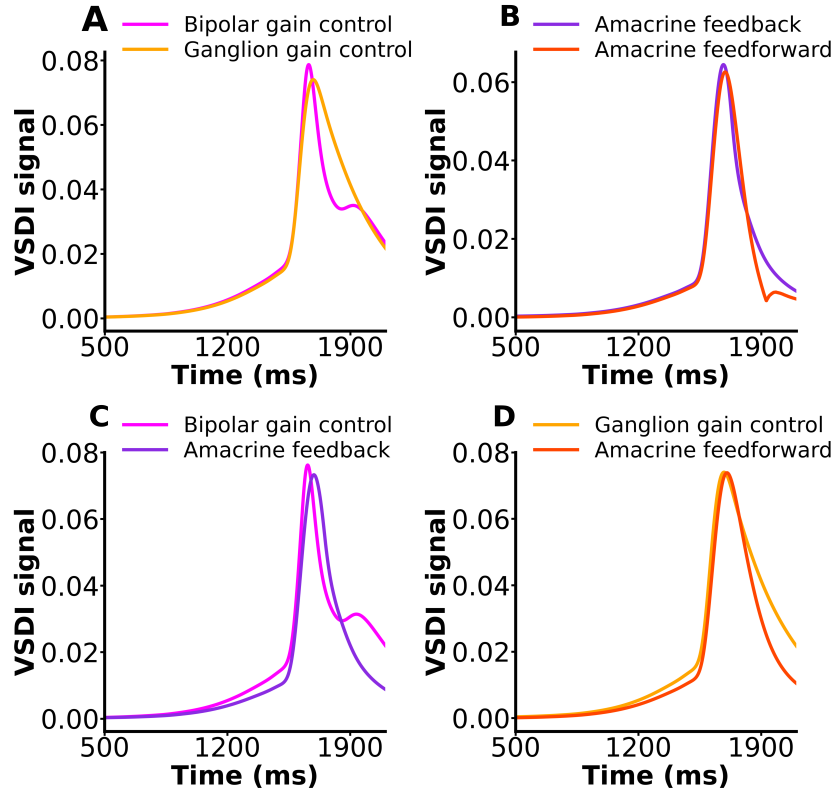


Figure 12: **Gain control and amacrine connectivity comparison.** **A)** Temporal profile of the VSDI response with a BC gain control  $h_B = 8.554$  mV/s (magenta) and a RGC gain control  $h_C = 0.359$  mV/s (yellow). **B)** Temporal profile of the VSDI response with amacrine feedback connectivity weight  $w_B^A = 11$  Hz (purple) and feedforward weight at  $w_C^A = 0.7$  Hz (orange). **C)** Temporal profile of the VSDI response with bipolar gain control  $h_B = 8.554$  mV/s (magenta) and amacrine feedback connectivity weight  $|w_B^A| = 11$  Hz (purple). **D)** Temporal profile of the VSDI response with ganglion gain control  $h_C = 0.359$  mV/s (yellow) and amacrine feedforward connectivity weight  $|w_C^A| = 0.7$  Hz (orange).

Fig. 12 C compares the BCs gain control to the ACs feedback still tuning the respective parameters so that the ROA are equal: BCs gain control  $h_B = 9.2$  mV/s and the feedback loop  $|w_B^A| = 9$  Hz (same ROA of 16.1 Hz). Considering the difference between AR in the BC gain control case and in the feedback connectivity case, we obtain a decrease of  $-8.4\%$ . This is  $-10.3\%$  for ML, and  $-4.9\%$  for SRAS, while SPD arises 36 ms later 55.2% and the intrinsic cortical SPD 3.4 ms (43%) after. In this example BCs gain control provides more anticipation with a visible effect on latency. Fig. 12 D compares as well the RGCs gain control to the ACs feedforward connectivity with  $h_C = 0.36$  mV/s,  $w_A^B = 0.6$  Hz (ROA equal to 17 Hz). We observe a decrease of  $-10.1\%$  for AR,  $-11.3\%$  for ML and  $-8.4\%$  for SRAS. The RGC SPD arises 17ms (18.1%) later and the cortical SPD 6ms (41.4%) later. For this set of parameters RGC gain control performs better than feedforward amacrine connectivity.

To sum up, this study provides an effective way of studying the potential impact of retinal anticipation mechanisms on cortical anticipation with a main drawback: parameters tuning. Although, the retinal model has been designed to have a minimal set of parameters (compared to a real retina) there are still quite a lot and a systematic study of the effects

requires actually an (ongoing) systematic mathematical analysis (Cessac-Ebert, in preparation). Note that numerical simulations do not allow to effectively sample the parameter space of the retina model, while a mathematical analysis shows that some parameters (such as  $\tau_A, \tau_B, w_B^A, w_A^B$ ) are actually dependent. Another alternative for parameter tuning would be experimental tests. Experiments on the retina somewhat allow one to tune these parameters so as to match empirical responses. But, as said in the introduction, they mainly hold for mice (or salamanders). A more efficient way and a bigger challenge would be to tune these parameters from the observation of the V1 VSDI signal, on the basis of this model and of the afferent simulation platform. We actually made in this paper a conjecture about the shape of the VSDI signal (presence of a rebound after the main peak) when, e.g., BCs gain control or ACs feedback connectivity is present. Their influence results in a measurable effect on the VSDI signal profile. It would be interesting to test these conjectures in new experiments.

In this spirit, we would like to come to the remark made in section 3.1. In CTL condition (without retinal anticipation) the anticipation by latency is a bit too high ( $-880$  ms for ML) compared to  $\sim -400, -600$  ms in Fig. 4D of [8] (where this range of variations comes from feedback effects). We have actually shown that adding a realistic retinal output has the effect of reducing the anticipation by latency in our model, in a range compatible with experimental observations (see e.g. Fig. 10 B). The same holds for the anticipation range which was  $6.3^\circ$  in CTL conditions compared to  $2^\circ$  in experiments. Again, the retina has the effect of reducing this discrepancy. To get better insights on the parameters values experiments could for example focus more on the VSDI shape (e.g. after the peak) and also investigate the effects of the bar speed on peak anticipation and latency anticipation.

## 4 Discussion

In this paper, we presented a chimera model connecting a multi-layered model of the retina to a mean-field model of V1. This allowed us to investigate how the retino-cortical pathway (where the thalamus-LGN was considered as a simple relay) can anticipate the trajectory of a moving object. Cortical anticipation is first manifested by a spatial gradient in the latency of the VSDI signal. This corresponds to a cooperative and cumulative non linear mechanisms where the cortical columns sensing the bar send information forward to pre-activate distant columns, generating what we called "anticipation by latency". In addition, we have exhibited an advancement of the VSDI signal peak, compared to the peak of the retinal ganglion cells that input cortical columns. We called this effect "anticipation by adaptation" or "anticipation by peak shift". Considering a simple retinal input (essentially an  $\alpha$ -drive as in [8]), with no anticipatory mechanism, we have shown that the amplitude of the retinal input or the stimulus contrast, as well as the length of lateral cortical connections, have a strong impact on the cortical anticipation by latency. We also studied the influence of the moving object speed where we gave evidence of a preferred speed where the anticipation by latency is maximal. In control conditions, the effects on the peak shift are quite smaller than the effects on latency.

We have then study cases where the retina actively cooperates with the cortex V1 to anticipate the trajectory. Essentially, the retina mechanisms that we have investigated (gain control and amacrine connectivity) induce a strong advancement of the retinal ganglion cell response peak, with a potential deformation of the whole retinal signal when the mechanism modulates the activity of bipolar cells. In the presence of retinal anticipation mechanisms, the retinal peak shifts forward and the response profile deformation generates entangled effects in the cortex. Not only the VSDI signal peak is advanced and is located at a position that matches experimental observations. Its whole shape is modified as well, leading to measurable and various effects on anticipation by latency. Depending on the control parameter value this can improve or decrease the anticipation range and the maximal latency, while the speed at which the anticipatory wave is propagating (short range anticipation speed) is a bit increased or stays constant. Although the mechanism of peak anticipation is known since long in the retina, [1], our work is the first, to our knowledge, showing how the effect of the peak offset in the retina is transmitted to the cortical response.

This study is far from being exhaustive though. First, a more extended study would require to vary the phenomenological parameters controlling such or such mechanism (e.g. the parameter  $h_B$  for bipolar gain control or the parameter  $\mu = -w_B^A w_A^B \tau^2$ , where  $\frac{1}{\tau} = \left| \frac{1}{\tau_B} - \frac{1}{\tau_A} \right|$  for feedback amacrine connectivity) along with the bar speed. Indeed, preliminary studies on the retina [13] have shown that acting on bipolar cells anticipation induces the existence of a speed range (preferred speeds) where anticipation by adaptation is maximum. What would be the effect on cortical anticipations ? Is there also a range of preferred speed, and do they correspond to physiological or psycho-physical observations ? Such an extensive study would also require to explore more deeply the set of parameters involved in the cortical model in future studies. As we briefly explained in the paper, this model exhibit pathological instabilities, when the retinal input increases too much. These instabilities can be controlled either by considering a so-called second order mean-field model [18, 23] or an adaptive mean-field model [24]. In particular the second order model introduces corrections in the Jacobian of the cortical model at the steady state. These corrections increase the value at which the retinal output amplitude triggers a Hopf bifurcation generating pathological oscillations. An important improvement

would also be to integrate a realistic thalamus in the model, that is, adding thalamic mean-field equations so as to design a mean-field model of the retino-thalamo (LGN)-cortical pathway [25]. Most excitatory synapses in the thalamus are of cortical origin [26], and thus the cortico-thalamic feedback, a feature not present in our model, is essential. In addition, thalamic neurons have very complex intrinsic firing properties, and can generate bursts of action potentials, so they are also not a simple relay. A future step would be to integrate these properties of the LGN by using a previously proposed model of the thalamus using AdEx neurons, which are formulated in mean-field [27] and integrated in our simulator. This would lead us to simulate the role of the thalamo-cortical loop not only for anticipation.

The retina model could be extended through an implementation of other cell types and more diverse types of connectivity, more realistic than nearest neighbours [22]. This would allow to implement more realistic retinal circuits, and assess their role in motion processing and anticipation. It would be in particular interesting to study the combined effect of gap junctions and amacrine cells connectivity, and assess whether their collaboration can improve cortical anticipation as suggested by [22].

The current implementation of our retino-cortical model takes as an input a set of images, processes them through the layered retina model in order to produce firing rates, which are then fed to the cortical model. It is hence possible to study the response of the model to different kind of 2D stimuli, and assess whether the mechanisms we have implemented for motion anticipation can also account for other visual effects. In particular is there anticipation on curved trajectories ? See [20] for preliminary results.

Finally, these results actually ask the question which features of the cortical activity profile (VSDI) are most used by the real brain to anticipate a trajectory: latency ? peak shift ? a combination of both ? or signal features that we didn't explore ? In [4] Menz et al observed a rise in the RGCs activity before a moving object enters their receptive field, advancing the *entire* retinal response (not only the peak), with a strong anticipatory effect. This response shift is called *predicting anticipation*. The authors hypothesized that this mechanism is due to the lateral inhibition by biphasic ACs, a feature that we didn't explore here. These cells have a first negative part of their activity that disinhibits BCs, followed by a second positive part that inhibits them. These two parts are relatively symmetrical and very close in amplitude. Sending such a signal to V1 would result in an increase in the early part of the peak and a similar reduction in the late part. This would result in a shift of the VSDI response arising earlier with a constant amplitude at the peak, since we have equivalent stimulation and inhibition. This opens up questions about how the various structure of the retina, with multiple cells sub-types and a large palette of synapses, contributes to motion anticipation and more generally to handling motion. In particular, the retina has the ability to detect surprise [28, 29, 30], e.g. an abrupt change in a trajectory. How is the surprise information transmitted to the visual cortex, how is it used, and how could it be measured? These are all interesting questions that could be explored in future studies.

**Acknowledgments.** This work was supported by the National Research Agency (ANR), in the project "Trajectory", <https://anr.fr/Project-ANR-15-CE37-0011>, funding Selma Souihel's PhD; the ANR too in the project "Shooting Star-15755" <https://anr.fr/Projet-ANR-20-CE37-0018>, funding Jérôme Emonet's PhD, and finally by the interdisciplinary Institute for Modelling in Neuroscience and Cognition (NeuroMod <http://univ-cotedazur.fr/en/idex/projet-structurant/neuromod>) of the Université Côte d'Azur. Mattéo Di Volo and Alain Destexhe are supported by the CNRS and the European Union (The Human Brain Project, H2020-945539). We thank O. Marre and S. Chemla for helpful discussions. We are grateful to the Service d'Etudes et Développement at Inria for helping develop the software Macular.

## 5 Appendix

### 5.1 Model parameters (default values)

Parameter category	Parameter Name	Symbol	Value	Unit
<b>Simulated area</b>	Number of cells (X)	$n_{cells_x}$	83	Dimensionless
	Number of cells (Y)	$n_{cells_y}$	15	Dimensionless
	Width (X)	$L_X$	18.45	degrees
	Height (Y)	$L_Y$	3.15	degrees
	Cell distance	$\delta$	0.225	degrees
	mm retina per degree	rpd	0.3	mm/degrees
	mm cortex per degree	cpd	3	mm/degrees
<b>Stimulus video (moving bar)</b>	Speed	$v_B$	6	degrees/s
	Width (X)	$l_X$	0.67	degrees
	Height (Y)	$l_Y$	0.9	degrees
	Frame rates	$\delta_t$	60	Hz
	Pixel per degree	$ppd$	300	pixel/degrees
<b>OPL</b>	OPL input amplitude	$C$	0.025	Dimensionless
	Integration time step (ODE solver)	$dt$	0.0004	s
	RF size	$\sigma_c$	0.2	degrees
<b>Bipolar cells</b>	Characteristic time	$\tau_c$	0.1	s
	Characteristic time	$\tau_B$	0.1	s
	Activity characteristic time	$\tau_{a_B}$	0.1	s
	Threshold	$\theta_B$	0	mV
<b>Amacrine cells</b>	Activity rate	$h_B$	[0,9.2]	$\text{mV}^{-1}\text{Hz}$
	Characteristic time	$\tau_A$	0.05	s
	Weight bipolar to amacrine	$w_A^B$	[0,12]	Hz
<b>Ganglion cells</b>	Weight amacrine to bipolar	$w_B^A$	[0,12]	Hz
	Weight amacrine to ganglion	$w_G^A$	[0,1]	Hz
	Radius bipolar to ganglion	$\sigma_G$	0.3	degrees
	Characteristic time	$\tau_G$	0.1	s
	Activity characteristic time	$\tau_{a_G}$	0.189	s
	Threshold	$\theta_G$	0	mV
	Activity rate	$h_G$	[0,0.54]	$\text{mV}^{-1}\text{Hz}$
<b>Cortical shared parameters values</b>	Weight bipolar to ganglion	$w_G^B$	0.15	Dimensionless
	Pooling extent	$\sigma$	0.09	mm
	Non linear rectification	$\alpha_G$	1110	Hz/mV
	Non linear rectification limit	$N_{G_{max}}$	212	Hz
	Membrane capacitance for cortical columns	$C_m$	0.2	nF
	Excitatory reversal potential	$V_E$	0	mV
	Inhibitory reversal potential	$V_I$	-80	mV
	Leak reversal potential	$V_L$	-65	mV
	Cell number in network	$N_{tot}$	10 000	Dimensionless
	Excitatory quantal conductance	$Q_E$	1.5	nS
	Leak conductance	$g_L$	10	nS
	Excitatory characteristic time	$\tau_E$	0.005	s
Inhibitory characteristic time	$\tau_I$	0.005	s	
External drive	$v_{ext}$	2	Hz	
Mean field characteristic time	$T$	0.005	s	
Fraction of inhibitory cells	$g_{ei}$	0.2	Dimensionless	

	Probability of connectivity	$p_{connec}$	0.0375	Dimensionless
	Mean voltage initial fit value	$\mu_V^0$	-60	mV
	Mean voltage initial fit variation	$\delta\mu_V^0$	10	mV
	Sigma initial fit value	$\sigma_V^0$	4	mV
	Sigma initial fit variation	$\delta\sigma_V^0$	6	mV
	Normalized tau initial fit value	$(\tau_V^N)^0$	0.5	Dimensionless
	Normalized tau initial fit variation	$(\delta\tau_V^N)^0$	1	Dimensionless
<b>Cortical excitators (RS)</b>	Sigma extent	$\sigma_E$	1.67	degrees
	Initial activity	$\nu_{E_0}$	1.86	Hz
	Inhibitory quantal conductance	$Q_I$	3	nS
	P parameters	$P_E$	[-49.8, 5.06, -25, 1.4, -0.41, 10.5, -36, 7.4, 1.2, -40.7]	mV
<b>Cortical inhibitors (FS)</b>	Sigma extent	$\sigma_I$	0.3	degrees
	Initial activity	$\nu_{I_0}$	12.66	Hz
	Inhibitory quantal conductance	$Q_I$	5	nS
	P parameters	$P_I$	[-51.4, 4, -8.3, 0.2, -0.5, 1.4, -14.6, 4.5, 2.8, -15.3]	mV
<b>Cortical column connectivity</b>	Retino-cortical amplitude	$w_{RC}$	2.5	Dimensionless
	Cortical density	$\rho_{cort}$	4000	$mm^{-2}$
	Retinal density	$\rho_{ret}$	400	$mm^{-2}$
	Fiber conduction velocity	$v_C$	300	mm/s
	Weight excitatory to excitatory	$A_E^E$	1	Dimensionless
	Weight inhibitory to inhibitory	$A_I^I$	1	Dimensionless
	Weight excitatory to inhibitory	$A_E^I$	1.5	Dimensionless
	Weight inhibitory to excitatory	$A_I^E$	1	Dimensionless

Table 1: **Model parameters.** For each parameter in our retino-cortical model, we give its name, symbol, unit and the default value used in control condition.

## 5.2 Mean-field cortical equations

We summarize here the mean-field equations derived in a series of paper [18, 11, 12, 17, 24, 31]. The goal is to propose dynamical equations characterising the average dynamics of the two populations of neurons, exciters and inhibitors, at the level of a cortical column. In the core paper, we have given the main equations ruling the dynamics. Here, we give more detail of their constitutive elements. For clarity we rewrite the dynamical equations (9), giving the evolution of the excitatory population rate,  $\nu_E(\vec{x}, t)$ , for the cortical column located at  $\vec{x}$  at time  $t$ , (resp.  $\nu_I(\vec{x}, t)$  for the inhibitory population rate), in the form:

$$\begin{cases} T \frac{\partial \nu_E(\vec{x}, t)}{\partial t} = -\nu_E(\vec{x}, t) + F_E [\mathcal{I}_E^E(\vec{x}, t), \mathcal{I}_E^I(\vec{x}, t)] \\ T \frac{\partial \nu_I(\vec{x}, t)}{\partial t} = -\nu_I(\vec{x}, t) + F_I [\mathcal{I}_I^E(\vec{x}, t), \mathcal{I}_I^I(\vec{x}, t)]. \end{cases} \quad (12)$$

where:

$$\begin{cases} \mathcal{I}_E^E(\vec{x}, t) = \nu^{aff}(\vec{x}, t) + \nu^{drive} + A_E^E \nu_E^{input}(\vec{x}, t), \\ \mathcal{I}_E^I(\vec{x}, t) = A_E^I \nu_I^{input}(\vec{x}, t), \\ \mathcal{I}_I^E(\vec{x}, t) = \nu^{aff}(\vec{x}, t) + \nu^{drive} + A_I^E \nu_E^{input}(\vec{x}, t), \\ \mathcal{I}_I^I(\vec{x}, t) = A_I^I \nu_I^{input}(\vec{x}, t). \end{cases} \quad (13)$$

Here,  $\mathcal{I}_X^Y(\vec{x}, t)$ ,  $X, Y = \{E, I\}^2$ , is the total contribution (firing rates) of population  $Y$  controlling the time evolution of population  $X$ .

Note a few important differences with the aforementioned papers. First, the retino-thalamic input  $\nu^{aff}$  is, in our case, acting on the two populations, excitatory and inhibitory. Also, we have introduced the coefficients  $A_X^Y$  weighting the relative contributions of excitatory and inhibitory populations,  $\nu_E^{input}$ ,  $\nu_I^{input}$ , from the other columns. These coefficients were implicitly set to 1 in these papers and, in this case,  $\mathcal{I}_E^E = \mathcal{I}_I^E$ ,  $\mathcal{I}_E^I = \mathcal{I}_I^I$  so that the superscript  $Y$  becomes useless.

We then define, dropping the  $(\vec{x}, t)$  dependence for legibility:

$$\mu_{G_X^Y} = \mathcal{I}_X^Y K_X \tau_X Q_X \quad (14)$$

$$\sigma_{G_X^Y} = Q_X \sqrt{\frac{\mathcal{I}_X^Y K_E \tau_X}{2}}; X, Y = \{E, I\}^2. \quad (15)$$

where,  $\mu_{G_X^Y}$  is contribution of population  $Y$  to the mean conductance of population  $X$  and  $\sigma_{G_X}$  the corresponding standard deviation, computed from shot-noise theory [32].  $K_E$  (resp.  $K_I$ ) is the number of excitatory synapses (resp. inhibitory),  $Q_E$  (resp.  $Q_I$ ) the unitary excitatory conductance (resp. inhibitory), and  $\tau_E$  (resp.  $\tau_I$ ) the excitatory decay (resp. inhibitory). See table in appendix 5.1 for the value of these parameters.

The total input conductance of the neuron  $\mu_G$  and its effective membrane time constant  $\tau_m^{\text{eff}}$  are controlled by the mean conductances as follows:

$$\begin{aligned} \mu_G &= \sum_{X, Y \in \{E, I\}^2} \mu_{G_X^Y} + g_L, \\ \tau_m^{\text{eff}} &= \frac{C_m}{\mu_G}, \end{aligned} \quad (16)$$

where  $C_m$  is the membrane capacitance, assumed to be the same for all neurons and  $g_L$  is the leak conductance.

The transfer functions of excitatory (resp. inhibitory) neurons appearing in eq. (12) take the form:

$$F_X(\mathcal{I}_E^X, \mathcal{I}_X^I) = \frac{1}{2\tau_{V,X}} \text{erfc}\left(\frac{\nu_{thr,X}^{eff} - \mu_{V,X}}{\sqrt{2}\sigma_{V,X}}\right), \quad X = E, I. \quad (17)$$

The quantity:

$$\mu_{V,X} = \frac{\sum_{Y=E,I} \mu_{G_X^Y} V_Y + g_L V_L}{\mu_G}, \quad X = E, I, \quad (18)$$

is the mean-voltage of the population  $X$  in the cortical column, where  $V_E, V_I, V_L$  are respectively the reversal potentials for excitatory (E), inhibitory (I) neurons and for the leak. Likewise:

$$\sigma_{V,X} = \sqrt{\sum_{Y=E,I} K_Y \mathcal{I}_X^Y \frac{(U_Y \tau_Y)^2}{2(\tau_m^{\text{eff}} + \tau_Y)}}, \quad (19)$$

$$\tau_{V,X} = \frac{\sum_{Y=E,I} (K_Y \mathcal{I}_X^Y (U_Y \tau_Y)^2)}{\sum_{Y=E,I} (K_Y \mathcal{I}_X^Y (U_Y \tau_Y)^2 / (\tau_m^{\text{eff}} + \tau_Y))}, \quad (20)$$

where we defined  $U_Y = \frac{Q_Y}{\mu_G} (V_Y - \mu_{V,Y})$  and where  $X = (E, I)$ .

Finally, in eq. (12),  $\nu_{thr,X}^{eff}$  is a phenomenological threshold expressed as a first order expansion (eq. (21)) of the three sub-threshold statistical quantities :  $\mu_{V,X}$ ,  $\sigma_{V,X}$ ,  $\tau_{V,X}$ . As it does not exist an analytic formulation of the transfer function for complex models such as the Adaptive Exponential IF or Hodgkin Huxley, Zerlaut et al. [11] have

developed a semi-analytic method based on a phenomenological threshold which carries the single neuron non-linearities mechanisms (spike/reset and adaptation). This leads to the following expression for the phenomenological threshold:

$$\nu_{thr,X}^{eff} = P_{X,0} + \sum_{u \in \{\mu_{V,X}, \sigma_{V,X}, \tau_{V,X}^N\}} P_{X,u} \cdot \left( \frac{u - u^0}{\delta u^0} \right) + \sum_{u,v \in \{\mu_{V,X}, \sigma_{V,X}, \tau_{V,X}^N\}^2} P_{X,uv} \cdot \left( \frac{u - u^0}{\delta u^0} \right) \left( \frac{v - v^0}{\delta v^0} \right), \quad (21)$$

where  $\tau_{V,X}^N = \tau_{V,X} G_l / c_m$  is an unitless parameter. Coefficients  $P_{X,u}$  have been fitted on numerical simulations of a given single AdEx neuron model with conductance-based exponential synapses [33]. Note that they are different for exciters and inhibitors. The value of these coefficients in our model are given in the table of appendix 5.1, as well as the coefficients  $\mu_V^0, \delta\mu_V^0, \sigma_V^0, \delta\sigma_V^0, (\tau_V^N)^0, (\delta\tau_V^N)^0$  which are actually assumed to be constant over the populations  $E, I$ .

Finally, the VSDI signal is given by:

$$VSDI(\vec{x}, t) = 0.8 \times VSDI_E(\vec{x}, t) + 0.2 \times VSDI_I(\vec{x}, t), \quad (22)$$

where the coefficient 0.8 and 0.2 corresponds to the fraction of exciters and inhibitors in the column population and:

$$VSDI_X(\vec{x}, t) = \frac{\mu_{V,X}(\vec{x}, t) - \mu_{V,X_0}(\vec{x})}{\mu_{V,X_0}(\vec{x})}, \quad X = E, I,$$

where  $\mu_{V,X_0}(\vec{x})$  is the average membrane potential at rest (i.e. when  $\nu^{aff} = 0$ , for the population  $X$ ). Note that it depends on  $\vec{x}$ , due to boundary conditions.

### 5.3 Connectivity type

Our retino-cortical model contains three different connectivity types :

- **One to one** connectivity link cells or cortical column populations with the same spatial position. This is the case for the connectivity from bipolar to amacrine or from ganglion cell to excitatory/inhibitory cortical column population.
- **Nearest neighbor + 1** connects a cells or cortical column with its 4 nearest adjacent cells or cortical columns. This is used to connect BCs to ACs and reciprocally.
- **Gaussian** connectivity connects the pre- and post-synaptic cell (column) with a weight proportional to a Gaussian function of the distance  $d_{[pre,post]}$  between the pre- and post-synaptic cell (eq. (11) in the text).

## References

- [1] M. Berry, I. Brivanlou, T. Jordan, and M. Meister, “Anticipation of moving stimuli by the retina,” *Nature*, vol. 398, no. 6725, pp. 334—338, 1999.
- [2] J. Johnston and L. Lagnado, “General features of the retinal connectome determine the computation of motion anticipation,” *Elife*, 2015.
- [3] S. Souihel and B. Cessac, “On the potential role of lateral connectivity in retinal anticipation,” *J. Math. Neurosc.*, vol. 11, no. 3, 2021.
- [4] M. D. Menz, D. Lee, and S. A. Baccus, “Representations of the amacrine cell population underlying retinal motion anticipation,” *bioRxiv*, 2020.
- [5] D. Jancke, W. Erlaghen, G. Schöner, and H. Dinse, “Shorter latencies for motion trajectories than for flashes in population responses of primary visual cortex,” *Journal of Physiology*, vol. 556, pp. 971–982, 2004.
- [6] G. Benvenuti, S. Chemla, A. Boonman, G. Masson, and F. Chavane, “Anticipation of an approaching bar by neuronal populations in awake monkey v1,” *Journal of Vision*, 2015.
- [7] M. Subramanian, A. S. Ecker, S. S. Patel, R. J. Cotton, M. Bethge, X. Pitkow, P. Berens, and A. S. Tolias, “Faster processing of moving compared with flashed bars in awake macaque v1 provides a neural correlate of the flash lag illusion,” *Journal of Neurophysiology*, 2018.
- [8] G. Benvenuti, S. Chemla, A. Boonman, L. Perrinet, G. S. Masson, and F. Chavane, “Anticipatory responses along motion trajectories in awake monkey area v1,” *bioRxiv*, 2020.
- [9] B. Cessac, “Retinal processing: Insights from mathematical modelling,” *Journal of Imaging*, vol. 8, no. 1, 2022.
- [10] E. Kartsaki, G. Hilgen, E. Sernagor, and B. Cessac, “How does the inner retinal network shape the ganglion cells receptive field : a computational study,” *Neural Computation*, vol. 36, pp. 1041–1083, June 2024.

- [11] Y. Zerlaut, S. Chemla, F. Chavane, and A. Destexhe, “Modeling mesoscopic cortical dynamics using a mean-field model of conductance-based networks of adaptive exponential integrate-and-fire neurons,” *Journal of Computational Neuroscience*, 2018.
- [12] S. Chemla, A. Reynaud, M. di Volo, Y. Zerlaut, L. Perrinet, A. Destexhe, and F. Chavane, “Suppressive traveling waves shape representations of illusory motion in primary visual cortex of awake primate,” *Journal of Neuroscience*, vol. 39, no. 22, pp. 4282–4298, 2019.
- [13] S. Ebert, *Dynamical synapses in the retinal network*. Phd thesis, Université Côte d’Azur, Dec. 2023.
- [14] E. Y. Chen, O. Marre, C. Fisher, G. Schwartz, J. Levy, R. A. da Silveira, and M. Berry, “Alert response to motion onset in the retina,” *Journal of Neuroscience*, vol. 33, no. 1, pp. 120–132, 2013.
- [15] S. Chemla, *A biophysical cortical column model for optical signal analysis*. PhD thesis, School of Information and Communication Sciences, 2010.
- [16] S. Chemla, F. Chavane, T. Vieville, and P. Kornprobst, “Biophysical cortical column model for optical signal analysis,” in *Sixteenth Annual Computational Neuroscience Meeting (CNS)* (W. R. Holmes, R. Jung, and F. Skinner, eds.), vol. 8, Suppl 2 of *BMC Neuroscience*, July 2007.
- [17] M. DiVolo, A. Romagnoni, C. Capone, and A. Destexhe, “Biologically Realistic Mean-Field Models of Conductance-Based Networks of Spiking Neurons with Adaptation,” *Neural Computation*, vol. 31, pp. 653–680, 04 2019.
- [18] S. ElBoustani and A. Destexhe, “A master equation formalism for macroscopic modeling of asynchronous irregular activity states,” *Neural computation*, vol. 21, no. 1, pp. 46–100, 2009.
- [19] R. Veltz, “An analytical method for computing Hopf bifurcation curves in neural field networks with space-dependent delays,” *Comptes Rendus Mathématique*, vol. 349, pp. 749–752, July 2011.
- [20] S. Souihel, *Generic and specific computational principles for visual anticipation of motion trajectories*. Phd thesis, Université Nice Côte d’Azur ; EDSTIC, Dec. 2019.
- [21] S. Souihel, B. Cessac, M. D. Volo, A. Destexhe, F. Chavane, S. Chemla, and O. Marre, “Anticipation in the retina and the primary visual cortex : towards an integrated retino-cortical model for motion processing,” in *NeuroMod 2019 - First meeting of the NeuroMod Institute*, (Fréjus, France), July 2019.
- [22] S. Souihel and B. Cessac, “Anticipation in the retina and the primary visual cortex : towards an integrated retino-cortical model for motion processing,” in *ICMNS 2019 - The 5th International Conference on Mathematical NeuroScience*, (Copenhagen, Denmark), June 2019.
- [23] D. Aquilué-Llorens, J. S. Goldman, and A. Destexhe, “High-Density Exploration of Activity States in a Multi-Area Brain Model,” *Neuroinformatics*, vol. 22, pp. 75–87, Jan. 2024.
- [24] M. Di Volo, A. Romagnoni, C. Capone, and A. Destexhe, “Biologically realistic mean-field models of conductance-based networks of spiking neurons with adaptation,” *Neural Computation*, vol. 31, pp. 653–680, Apr. 2019.
- [25] J. Overwiening, F. Tesler, D. Guarino, and A. Destexhe, “A multi-scale study of thalamic state-dependent responsiveness,” *bioRxiv*, 2024.
- [26] S. Sherman and R. Guillery, “Distinct functions for direct and transthalamic corticocortical connections,” *J Neurophysiol.*, vol. 106, no. 3, pp. 1068–77, 2011.
- [27] A. Destexhe, “Self-sustained asynchronous irregular states and up-down states in thalamic, cortical and thalamocortical networks of nonlinear integrate-and-fire neurons,” *J Comput Neurosci.*, vol. 27, no. 3, pp. 493–506, 2009.
- [28] G. Schwartz, R. Harris, D. Shrom, and M. J. Berry, “Detection and prediction of periodic patterns by the retina,” *Nature Neuroscience*, vol. 10, no. 5, pp. 552–554, 2007.
- [29] S. Ebert, T. Buffet, B. Sermet, O. Marre, and B. Cessac, “Temporal pattern recognition in retinal ganglion cells is mediated by dynamical inhibitory synapses,” *Nature Communication*, vol. 15, p. 6118, 2024.
- [30] D. Despotović, C. Joffrois, O. Marre, and M. Chalk, “Encoding surprise by retinal ganglion cells,” *PLOS Computational Biology*, vol. 20, no. 4, pp. 1–20, 2024.
- [31] M. DiVolo and I. M. Férézou, “Nonlinear collision between propagating waves in mouse somatosensory cortex,” *Scientific Reports*, vol. 11, p. 19630, 2021.
- [32] A. Papoulis, *Probability, Random Variables and Stochastic Processes*. McGraw-Hill, New York, 1965.
- [33] M. Carlu, O. Chehab, L. Dalla Porta, D. Depannemaecker, C. Héricé, M. Jedynek, E. Köksal Ersöz, P. Muratore, S. Souihel, C. Capone, Y. Zerlaut, A. Destexhe, and M. Di Volo, “A mean-field approach to the dynamics of networks of complex neurons, from nonlinear Integrate-and-Fire to Hodgkin-Huxley models,” *Journal of Neurophysiology*, vol. 123, pp. 1042–1051, Mar. 2020.